AN OBSTACLE-CONTROLLED CREEP MODEL FOR SN-PB AND SN-BASED LEAD-FREE SOLDERS

Appeared in Proceedings, SMTA International Conference (SMTAI '04), Sept. 26-30, 2004, Chicago, IL.

Jean-Paul Clech
EPSI Inc.
Montclair, NJ 07042, USA
jpclech@aol.com

ABSTRACT

This paper presents the application of physically-based, obstacle-controlled creep models to the analysis of steady-state creep rates for eutectic SnPb and seven lead-free solders: Sn58Bi, Sn0.7Cu, Sn3.5Ag, Sn4Ag, Sn3.8Ag0.7Cu, Sn3.5Ag0.75Cu and Sn2.5Ag0.8Cu0.5Sb. Lead-free, Sn-based solders are amenable to such models since dispersed intermetallics, grain boundaries, the lattice of the tin matrix itself and other dislocations, are all obstacles that impede dislocation motions. The basic single-cell, obstacle-controlled creep model, after Frost and Ashby (1982), features a stress-dependent activation energy and an athermal flow strength parameter which represents the maximum flow strength of the material at the absolute zero (0 Kelvin). Depending on how many creep mechanisms have been identified, the solder creep model is formulated as a single- or double-cell model. In the latter case, creep rates for the two mechanisms are additive. For each alloy, one set of steady-state creep measurements is used to determine the scaling constants and the physical parameters of the model (4 or 8 constants in total for the single- or two-cell models, respectively). Each model is then tested against independent test results (as many as nine test cases for the Sn3.5Ag alloy).

The obstacle-controlled, solder creep models allow for the bridging of tension, compression and shear test results as well as that of creep, strength and stress relaxation data, often without, and sometimes with the use of a simple, multiplicative calibration factor. The models also allow for the prediction of solder joint stress/strain measurements during thermal cycling of soldered assemblies. The need for calibration factors suggests that creep models derived from a given mechanical test, and specimen type or size, should not be used without justification in the stress/strain analysis of soldered assemblies. Model calibration and validation is a critical step in the application of creep models to stress analysis or reliability models.

The use of obstacle-controlled creep models resolves many anomalies observed in the classical analysis of lead-free solder creep data, including activation energies and power-law exponents that were found to be stress- and/or temperature-dependent. In accord with experts who warned against the use of power-law and hyperbolic sine creep models for engineering metals, we recommend caution when using such models for stress or reliability analysis of lead-free assemblies. As demonstrated by bouncing the models in this paper against many independent datasets, obstacle-controlled creep models offer a promising alternative.

Using the two-cell creep models, creep contour charts were generated to quantify the contribution of competing creep mechanisms to the total creep rates. The patterns of creep contour lines are quite different for Sn37Pb and Sn3.8Ag0.7Cu, a reflection of vastly different creep mechanisms. The Sn3.Ag0.7Cu creep contour chart suggests a transition from one mechanism to another that is highly temperature related. The transition occurs at about 75°C, in agreement with microstructural and creep rate analysis conducted by Vianco et al. (2004) on Sn3.9Ag0.6Cu solder.

Key words: SnPb, SnBi, SnAg, SnCu, SnAgCu, lead-free solder, obstacle-controlled creep models, stress dependent activation energy, creep mechanism contour charts.

INTRODUCTION

One of the challenges facing design engineers is the selection of relevant constitutive models to describe the creep behavior of solder in solder joints of real assemblies. This process has huge implications since it will impact the accuracy of ensuing stress analysis and reliability evaluations for soldered board assemblies. Creep being a significant deformation mode for Sn-based solders, it is critical that its stress, time and temperature dependence be modeled in a reasonably accurate manner. Excellent creep data has been produced over the years, providing insight into creep rates and mechanisms for a variety of solders. The apparent disparity in the data relates in part to the many variables that affect the microstructure, including alloy composition, process and ageing conditions, specimen geometry and test configuration. While our ultimate objective is to develop full fledge constitutive models for the development of lead-free acceleration factors and life prediction models, this paper is limited to the analysis of steady-state creep data. Primary creep and creep rupture deserve as much attention but are beyond the scope of the present study.

Emphasis is on lead-free solders and SnPb is included in the analysis for comparison purposes. The first part of the paper compares SnPb and lead-free solder creep data in an attempt to put a large number of test results in perspective. The second part, which is the bulk of the paper, describes the development and validation of steady-state creep models for a variety of Sn-based solders. Based on anomalies that have been observed in the application of classical creep models - power-law or hyperbolic sine models – to Pb-free solders, the analysis focuses on the development of obstacle-controlled creep models derived from the physically-based, rate-dependent plasticity models described by Frost and Ashby (1982).

COMPARISON OF SN-PB AND LEAD-FREE CREEP DATA

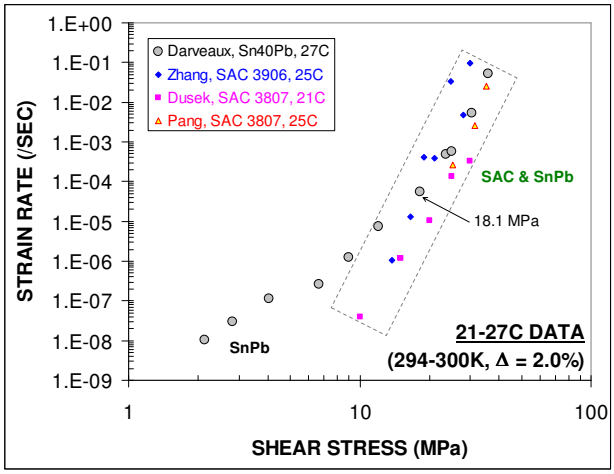

(a) Shear creep data at about 25℃

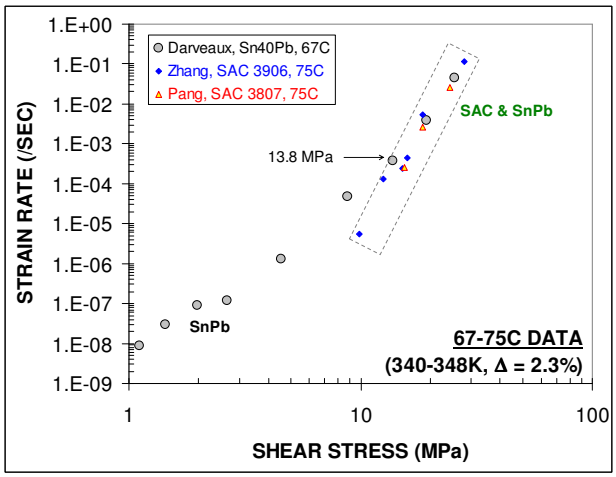

(b) Shear creep data at about 75°C

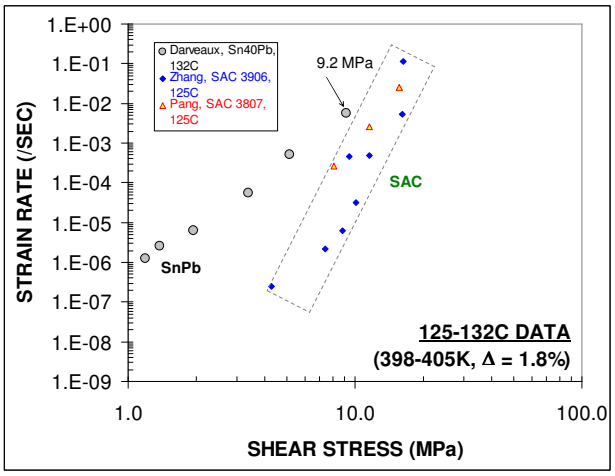

(c) Shear creep data at about 125℃

Figure 1: Isothermal steady-state creep rates in shear for standard SnPb and several lead-free solders.

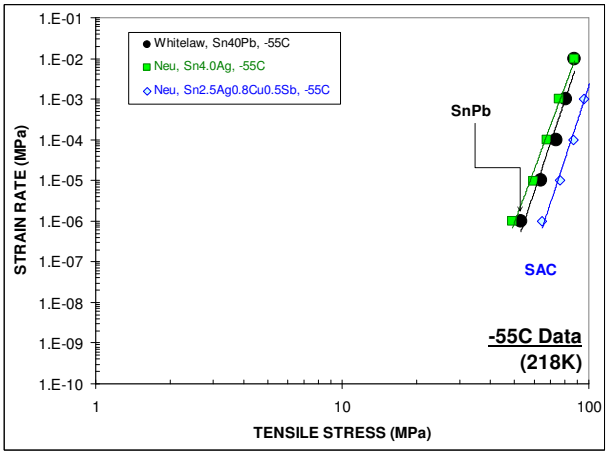

(a) Tensile creep data at -55℃

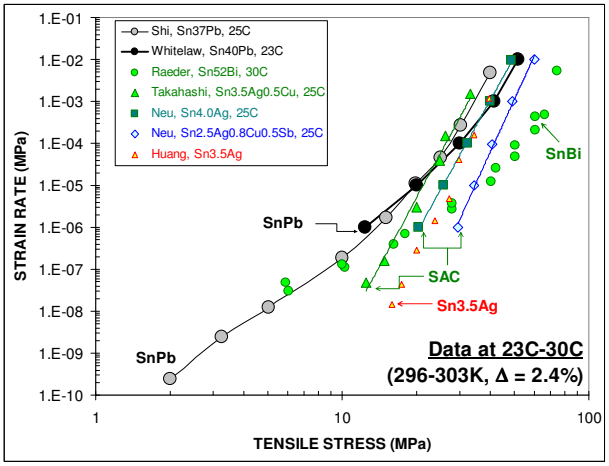

(b) Tensile creep data at about 25°C

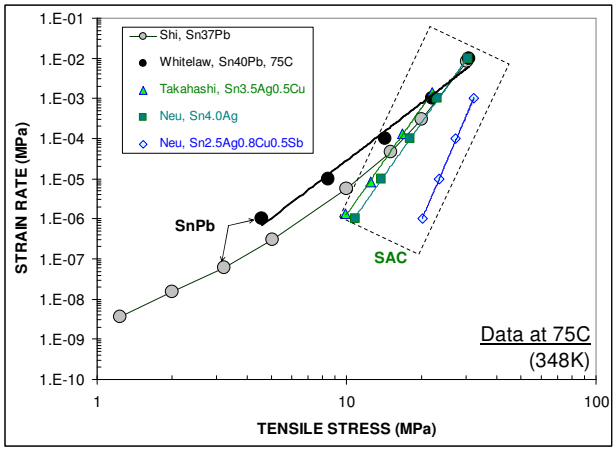

(c)Tensile creep data at 75°C

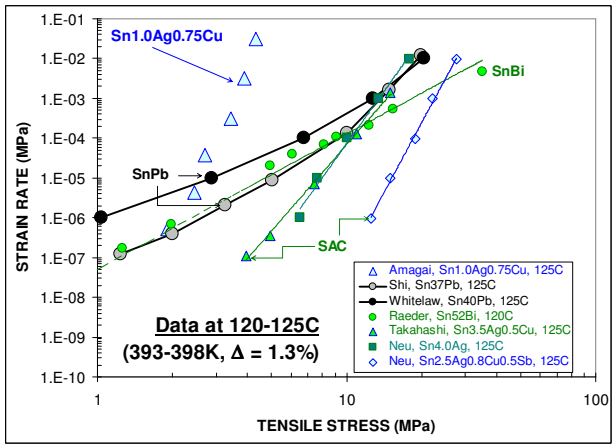

(d) Tensile creep data at about 125°C

Figure 2: Isothermal steady-state creep rates in tension for standard SnPb and several lead-free solders.

A myth seems to persist that Sn-Ag-Cu solder is always more creep resistant than standard SnPb. While this is true under low enough stress, creep rates are often more similar under high stress conditions as in harsh environments or under accelerated testing conditions. A cursory look at steady-state creep data (Figures 1 and 2) for SnPb and lead-free solders suggests that, over a wide temperature range, -55°C to 125°C, and under high enough stress, many of the common lead-free solders - except perhaps for eutectic SnBi - creep at similar rates or faster than standard SnPb. Schubert et al. (2002) arrived at a similar conclusion. Figures 1 and 2 are plots of isothermal steady-state creep data in shear and tension, respectively, for near-eutectic SnPb and lead-free solders of various compositions. The data in Figures 1 and 2 is from references with first authors listed in the legends. The shear data in Figures 1a through 1c is at test temperatures of about 25°C, 75°C and 125°C, respectively. The tensile data in Figures 2a through 2d is at temperatures of about -55°C, 25°C, 75°C and 125°C, respectively. When temperatures were not quite the same on a given plot (Figures 1 and 2), the temperature range on the absolute scale (degree Kelvin) was small, with temperature differences, Δ, of at most 2.4%.

From the data in Figure 1, shear creep rates for SAC alloys of composition Sn3.8Ag0.7Cu or Sn3.9Ag0.6Cu are similar to creep rates for Sn40Pb, starting at stress levels in the range 10 MPa to 20MPa. For the tensile data in the temperature range 25-125°C (Figures 2b-d), creep rates for the lead-free solders are similar or higher than for SnPb starting at a stress level of about 10 MPa. The transition stress is much lower, at about 2-3 MPa, for the Sn1.0Ag0.75Cu alloy with reduced Ag contents. At -55°C (Figure 2a), the creep rates for Sn40Pb are slightly higher than but quite similar to creep rates for Sn4.0Ag. The transition in relative creep rates, with similar or higher rates for common SAC alloys than for SnPb under high stress conditions, can possibly explain shorter solder joint lives experienced by SAC alloys, compared to SnPb solder, under highly accelerated conditions and large cyclic shear strains (Clech, 2004).

In Figures 2b (25°C) and 2d (125°C data), eutectic SnBi appears to be consistently more creep resistant than eutectic SnPb under high stress conditions. At lower stress, creep rates for the two eutectic alloys are very similar. The rather good creep resistance of eutectic SnBi at all stress levels is consistent with the thermal cycling test results of the National Center for Manufacturing Sciences (NCMS, 1997) lead-free project where SnBi surface-mount assemblies outperformed SnPb assemblies under two thermal cycling conditions, 0°C to 100°C and -55°C to 125°C.

STEADY-STATE CREEP MODELS

POWER-LAW AND "SINH" MODELS

Two convenient models in the study of steady-state creep of SnPb and lead-free solders are the power-law model and the hyperbolic sine ("sinh") model. In their simplified form, the two models are given as:

$$\dot{\varepsilon} = A\sigma^m \cdot \exp(-Q_a/kT) \qquad (1a)$$

$$\dot{\varepsilon} = A'[\sinh(B \cdot \sigma)]^n \cdot \exp(-Q_a/kT) \qquad (1b)$$

where the strain rate $\dot{\varepsilon}$ is a function of stress, σ, and absolute temperature, T. k is Boltzmann's constant (8.63 x 10^{-5} eV/K), A, A' and B are scaling parameters, and m and n are stress function exponents. The apparent activation energy, Q_a, for the controlling creep mechanism is assumed to be constant. Both models also assume that steady-state creep rates are dictated by a single creep mechanism over the stress and temperature range of interest. The "sinh" model offers the mathematical convenience of capturing changes of slopes in plots of strain rate versus stress data. A single-cell "sinh" model, as given by equation (1b) or an equivalent formulation where stresses are scaled by the shear modulus of the material, includes one activation energy, implying that only one creep mechanism is present.

When two creep mechanisms are identified, the power-law model is sometimes generalized as an additive, two-cell model:

$$\dot{\varepsilon} = A_1\sigma^{n_1} \cdot \exp(-Q_{a,1}/kT) + A_2\sigma^{n_2} \cdot \exp(-Q_{a,2}/kT) \quad (2)$$

where subscripts 1 and 2 refer to parameters for the two dominant creep mechanisms.

The above models have been applied to SnPb and lead-free solders with various degrees of success. Pao (1997) found a strong temperature dependence of power-law exponents for Sn3.5Ag solder. Shi et al. (2002) showed that the application of the power-law model to eutectic SnPb leads to a stress exponent and an activation energy that vary with stress and/or temperature, thus suggesting a new constitutive model with stress and temperature-dependent activation energy. Song et al. (2002 a & b) also observed a strong and systematic temperature dependence of stress exponents, and stress-dependent activation energies, for four lead-free solders: Sn3.5Ag, Sn3Ag0.5Cu, Sn0.7Cu and Sn-10In-3.1Ag. The situation was described as "*anomalous creep in Sn-rich solder joints*". The different temperature dependence of stress exponents in the low and high stress regions of the creep tests by Song et al. (2002 a & b) suggest that even a two-cell power-law model - equation (2) - is not applicable to lead-free solders.

The "sinh" model has also been used extensively in the analysis of Sn-Ag-Cu (SAC) solder creep data. This has led to widely different values of creep activation energies across the literature as well as differences in activation energies in tension and shear (Clech, 2004a). Vianco (2004) showed that, to a first order, the "sinh" model fits SAC compression creep rates when the data is divided into two temperature ranges, -25°C to 75°C and 75°C to 160°C, leading to two separate models with different activation energies above and below 75°C. Wiese et al. (2001, 2003) used a "sinh" model to fit bulk Sn-Ag-Cu solder creep data but pointed out that the model could not predict creep rates for flip-chip solder joints. The Sn-Ag-Cu flip-chip creep data appeared to fit a power-law model with a high exponent of 18. Clearly, the application of one- or two-cell power-laws or "sinh" models to steady-state creep of lead-free solder has been unsatisfactory. Their applicability to stress analysis of, or reliability modeling of solder joints in lead-free assemblies should be taken with a grain of salt.

According to experts in creep of metals, the power-law and "sinh" models lack a physical basis and do not provide a reliable indication of dominant creep mechanisms:

- "*UNFORTUNATELY, THESE POWER-LAW APPROACHES HAVE NEVER BEEN ADEQUATE DESCRIPTIONS OF PRACTICAL MATERIALS*", Bhadeshia et al. (2003).

- "*FOR OVER HALF A CENTURY, RELIANCE ON POWER-LAW APPROACHES HAS FAILED TO CLARIFY THE MECHANISMS GOVERNING CREEP STRAIN ACCUMULATION..., EVEN IN PURE MATERIALS*", Wilshire (2003) as quoted in Bhadeshia et al. (2003).

- "*DESPITE BEING WIDELY ADOPTED FOR OVER 50 YEARS, POWER-LAW CONCEPTS HAVE NOT LED TO THEORIES WITH VERIFIED PREDICTIVE CAPABILITIES...IT IS, THEREFORE PROPOSED THAT POWER-LAW REPRESENTATION OF STEADY STATE CREEP RATES SHOULD BE ABANDONED...*", Wilshire (2002).

- Referring to the "sinh" model parameters: n' = n and α' such as α' / μ = B in equation (1b), with μ being the shear modulus of the material, Frost and Ashby (1982) state: "*LACKING ANY PHYSICAL MODEL, IT MUST BE CONSIDERED FORTUITOUS THAT ANY SET OF n' AND α', CAN CORRECTLY DESCRIBE THE BEHAVIOR OVER A WIDE RANGE OF STRESSES*".

The empirical convenience of one- or two-cell power-law or "sinh" models has been a useful approximation and seems to have worked well in solder joint reliability studies of standard SnPb assemblies – see, for example, Clech, '96, '98, '00, '04 and Darveaux, 2002. A fundamental weakness of single-cell "sinh" models remains in that the representation of the data with a single Arrhenius factor does not reflect the activation energies of the two known creep mechanisms of near-eutectic SnPb, namely, grain boundary sliding and matrix creep with the activation energy for the first mechanism being about half that for matrix creep. The advent of lead-free solders provides an opportunity to revisit old concepts and develop improved approaches based on more physically-based constitutive models.

OBSTACLE-CONTROLLED CREEP MODELS

Sn-based solders consist essentially of a Sn matrix in which other phases and/or precipitates - small or large - are embedded. Deformations are limited by discrete obstacles distributed throughout the lattice. The lattice itself offers resistance to dislocation motions. Phases, precipitates, grain boundaries and other defects, including other dislocations, all constitute obstacles to dislocation motion. Under those conditions, this paper investigates the applicability to solder alloys of rate-dependent, obstacle-controlled plasticity models as described in Frost and Ashby (1982). Using the simplest version of Frost and Ashby's models, and for a single dominant creep mechanism, we suggest the following formulation of single mechanism, steady-state creep rates for Sn-rich solders:

$$\dot{\varepsilon} = A\sigma^m \cdot \exp\left[-\frac{Q_a}{kT}\left(1-\frac{\sigma}{\sigma_0}\right)\right] \qquad (3)$$

Besides the stress exponent m and the apparent activation energy Q_a – as in power-law creep – the obstacle-controlled creep model includes a maximum flow stress or athermal flow strength parameter, σ_0. This maximum flow stress σ_0 is interpreted as a maximum strength at a temperature of zero on the absolute scale, or as the strength in the absence of thermal energy. According to Frost and Ashby, σ_0 "*reflects not only the strength but also the density and arrangement of the obstacles*". The theoretical value of the stress exponent m is 2 for rate-dependent plasticity in a lattice with small discrete obstacles. Its value can be higher for more complex situations as in the case of creep of dispersion-strengthened alloys. From equation (3), the generalized form of the Arrhenius factor would capture the linear stress-dependence of the true activation energy: $Q = Q_a \cdot \left(1-\frac{\sigma}{\sigma_0}\right)$ as was verified experimentally for eutectic SnPb (Shi et al., 2002). The true activation energy is sometimes written as: $Q = Q_a - V \cdot \sigma$, where V is an apparent activation volume. In the latter formulation, Q shows distinct thermal and mechanical components to indicate that creep is a thermally activated, stress-aided rate process.

In most Sn-based solders, loads are carried by the bulk matrix - with or without strength-enhancing precipitates - and/or the most critical grain boundaries. The dominant deformation modes are some type of, or a combination of Matrix Creep (MC) and Grain Boundary Creep (GBC), depending on stress and temperature. The actual creep mechanisms are determined on a case-by-case basis:

- For eutectic SnPb, the matrix is the Sn-rich network phase. For SnBi, the Sn-rich matrix is reinforced by small, round Bi particle precipitates that form near the eutectic temperature where Bi is soluble in Sn. In both cases, the MC component of creep captures deformations of the Sn-rich phase. For SnPb, the GBC component describes Grain Boundary Sliding (GBS), in agreement with established creep mechanisms for standard SnPb.

- For Sn-Ag and Sn-Ag-Cu solders, the matrix is the inter-dendritic, quasi-eutectic network phase. The MC component of creep refers to deformations within the inter-dendritic Sn-rich phase that is strengthened by Ag_3Sn and/or Cu_6Sn_5 precipitates or particles. For Sn3.5Ag, grain boundary creep refers to some type of strain relief, decohesion or cracking at grain interfaces, in particular interfaces containing Ag_3Sn particles/precipitates (Rhee et al., 2003).

When two distinct creep mechanisms are present, we suggest a two-cell, obstacle-controlled creep model:

$$\dot{\varepsilon} = A_1\sigma^{m_1} \cdot \exp\left[-\frac{Q_{a1}}{kT}\left(1-\frac{\sigma}{\sigma_{01}}\right)\right] + A_2\sigma^{m_2} \cdot \exp\left[-\frac{Q_{a2}}{kT}\left(1-\frac{\sigma}{\sigma_{02}}\right)\right] \qquad (4)$$

where subscripts 1 and 2 refer to the two dominant creep mechanisms. The steady-state creep model described by equations (3) or (4) is for one or two primary deformation modes although it can potentially be extended to more. In (4), the total strain rate is given as the sum of two rates, with each component having an activation energy that corresponds to a given creep mechanism. The single-cell model – equation (3) – has four parameters as does the "sinh" model. The two-cell model - equation (4) - has a total of eight constants. All parameters are alloy-dependent and are obtained by fitting equation (3) or (4) to test data. A non-linear regression procedure, also known as curve-fitting, is used that converges more easily when the physical parameters are initialized to realistic values. The tool we used is a non-linear regression program by Oakdale Engineering. Because strain rates are low and cover several orders of magnitude, the regression is done using $Y = \ln(\dot{\varepsilon})$ as the response variable and $X_1 = T$ and $X_2 = \sigma$ as independent variables. Recommendations are given later for initial estimates of the physical parameters, an important but rarely discussed aspect of constitutive model development. The implementation of the obstacle-controlled model is worked out by examples with emphasis on the interpretation of model parameters and model validation. Alloy-specific models are tested by comparison to independent test results. Model testing is a critical aspect of constitutive model development although this does not appear to be a common practice in the solder mechanics literature.

APPLICATION TO EUTECTIC SN-PB SOLDER

EUTECTIC SN-PB MODEL

Using a non-linear regression program, equation (4) is fitted to 63Sn37Pb steady-state, tensile creep data by Shi et al. (2002). We chose a two-cell model since eutectic SnPb is known to have two main creep mechanisms, matrix creep and grain boundary sliding. The data in Figure 2 in Shi et al. (2002) was presented as shear creep data and was reconverted to the original tensile values using the Von Mises transformation between shear and tensile stress and strain rate: $\tau = \sigma/\sqrt{3}$ and $\dot{\gamma} = \dot{\varepsilon}\sqrt{3}$.

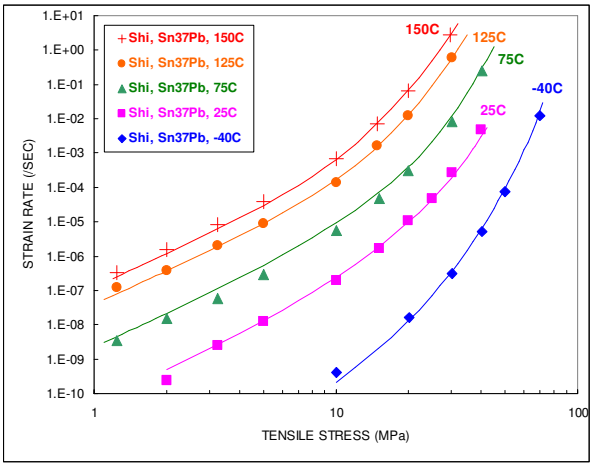

Figure 3: Eutectic SnPb, steady-state tensile creep data (symbols) from Figure 2 in Shi et al., 2002, and fit of two-cell, obstacle-controlled creep model (solid lines).

The equation of the solid lines in Figure 3 is:

$$\dot{\varepsilon}(/\sec) = 17.4\sigma^{3.07} \cdot \exp\left[-\frac{7988}{T(K)}\left(1-\frac{\sigma}{171}\right)\right] + 5112\sigma^{5.89} \cdot \exp\left[-\frac{13516}{T(K)}\left(1-\frac{\sigma}{217}\right)\right] \quad (5)$$

where the tensile stress σ has units of MPa and the temperature T is in degree Kelvin. The first term in (5) corresponds to grain boundary creep with an apparent activation energy: Q_{a1} = 7988 K x 8.314 J/(K. mole) = 66.4 kJ/mole or Q_{a1} = 7988 K x (8.63 x 10^{-5} eV/K) = 0.69 eV. The latter value is the same as an activation energy of 0.69 eV for grain boundary creep in Baker (1979) and is 38% higher than an activation energy of 0.5 eV in Grivas et al. (1979) under high strain rate conditions. The second term in (5) represents matrix creep with an apparent activation energy Q_{a2} = 112 kJ/mole = 1.17 eV, slightly higher than an activation energy of about 1 eV for tin self-diffusion.

The central values and standard errors for the parameters in equation (5) are:

- Q_{a1} = 66.4 ± 1.45 kJ/mole; m_1 = 3.07 ± 0.12; σ_{01} = 171 ± 8 MPa
- Q_{a2} = 112 ± 11 kJ/mole; m_2 = 5.89 ± 1.18; σ_{02} = 217 ± 54 MPa
- A_1 = 17.4 ± 8.1 ; A_2 = 5112 ± 24831

The scaling constants A_1 and A_2 have the largest standard errors, which is not unique to the type of model being used and would happen as well with scaling constants of "sinh" models. The reason for this is that the data spans several orders of magnitude on the creep rate axis. Nevertheless, the correlation coefficient for fitting equation (4) to the 40 observation points in Figure 3 is high: r^2 = 99.7%. Initial values of parameters in the regression program were set based on average literature values for power-law parameters for the two known creep mechanisms: m_1 ~ 3, m_2 ~ 7, Q_{a1} ~ 0.5 eV, Q_{a2} ~ 1 eV. For the athermal flow strength, we entered values based on the largest Ultimate Tensile Strength (UTS) that could be found in the literature: σ_{01} = σ_{02} = 144 MPa for eutectic SnPb at -200℃ (73K) at a moderately high strain rate of 3 x 10^{-3}/sec in Jones et al. (1998). As expected, the results for the athermal flow strength parameters are higher than the above UTS of 144 MPa at -200℃.

MODEL TESTING

Comparison to 60Sn40Pb Tensile Creep Data

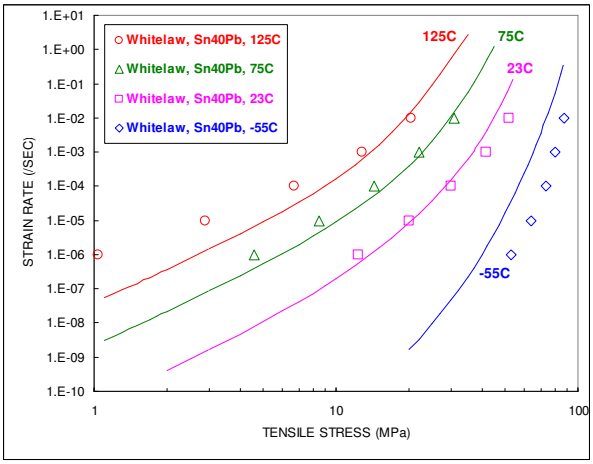

Figure 4: Fit of 63Sn37Pb two-cell model (lines) to 60Sn40Pb creep data (symbols, from Figure 3b in Whitelaw et al., 1999).

One important steps in constitutive model development is to bounce models against independent data in order to test the applicability and the limits of validity of a given model. In Figure 4, we have plotted steady-state creep data for 60Sn40Pb from Whitelaw et al. (1999). The lines represent the 63Sn37Pb two-cell creep model - equation (5) with no calibration factor - at -55℃, 23°C, 75°C and 125°C. The data follows the general trends of the model although the model is offset from the -55℃ data by about one order of magnitude. The overall fit is fairly good given the significant variability of creep rate measurements, possibly by one or two orders of magnitude. Slight differences in alloy composition as well as more marked differences in test specimens and conditions, as shown in Table 1 (at the end of the paper), may also explain the imperfect fit of the 63Sn37Pb creep model to the 60Sn40Pb data.

Comparison to 60Sn40Pb Compressive Stress Relaxation Data

Figures 5a and 5b show 60Sn40Pb compressive stress relaxation data from Baker et al. (1973) for two values of the initial stress and temperatures in the range 27℃ to 108℃. The solid lines are predictions obtained by using the creep model in equation (5) for 63SnPb with a creep rate calibration factor: C = 9 x 10^{-3} (almost 1/100).

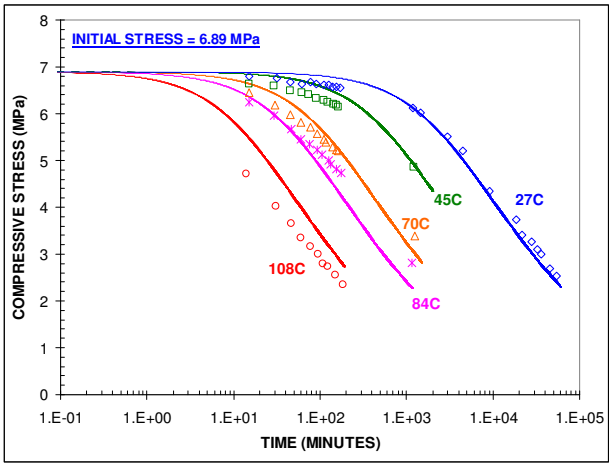

(a)

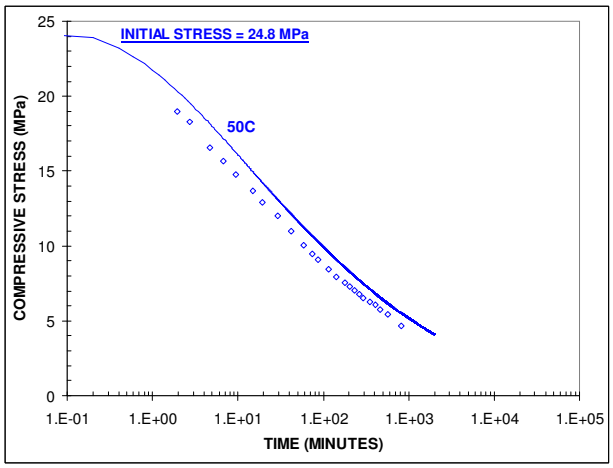

(b)

Figure 5: Prediction (solid lines) of 60Sn40Pb compressive stress relaxation using the 63Sn37Pb two-cell, creep model with a calibration factor C = 9 x 10^{-3}. The 60Sn40Pb stress relaxation data (symbols) is from Figures 3 and 6 in Baker et al., 1973.

In an isothermal stress relaxation test, the total strain is constant. Assuming that the total strain is the sum of elastic and creep strains, and neglecting machine and fixture stiffness, the solder stress response is determined from the strain rate equation (6a):

$$\frac{\dot{\sigma}}{E} + \dot{\varepsilon}_c = 0 \qquad (6a)$$

or $$\Delta\sigma = -E \times \dot{\varepsilon}_c \times \Delta t \qquad (6b)$$

where $\dot{\sigma}$ is the stress rate, $\dot{\varepsilon}_c$ is the creep rate and E is Young's modulus of solder at a given temperature. For a given value of the initial stress, and using time-steps, Δt, that are small enough, equation (6b) allows for the computation of stress increments Δσ at the end of each time step. The stress-relaxation lines in Figure 5 were obtained by implementing equation (6b) in a spreadsheet. For 63Sn37Pb, we used the temperature-dependent Young's modulus (Knecht et al., 1991): E(T) = 32-0.088*T(℃) in units of GPa. For $\dot{\varepsilon}_c$, which is computed at the beginning of each time interval, we used the tensile creep rate equation for 63Sn37Pb - right hand-side of equation (5) - times a calibration factor C. Using C = 9 x 10^{-3}, we obtained a visual best fit to the data in Figure 5a. We then used the same value of the calibration factor to predict the stress relaxation line in Figure 5b for a higher value of the initial stress.

The stress relaxation lines in Figures 5a and 5b follow measured stresses with an error of at most 20% over a test period as long as 1000 hours. The model also captures the temperature dependence of the data closely. The calibration factor C = 9 x 10^{-3}, close to 1/100, indicates that, when comparing the test results of Shi et al. (2002) and Baker et al. (1973), creep rates had to be scaled by about two orders of magnitude. This can be explained by differences in microstructures, which arise, from test specimens and conditions, as summarized in Table 2, as well as a possibly uneven behavior of near-eutectic SnPb in compression and in tension. The fact that we had to use a calibration factor to get the right order of magnitude of stresses suggest that creep rates based on mechanical testing of laboratory specimens may have to be scaled before they can be applied to the modeling of solder joints of electronic assemblies.

Prediction of 60Sn40Pb Ultimate Tensile Strength

Figure 6a shows UTS data for eutectic SnPb as a function of temperature in the range -200℃ to 150°C. The data in Figure 6b is from tensile tests run at different strain rates. Test and specimen conditions are summarized in Table 3. For a given strain rate, and at a given temperature, we obtained strength values by back solving equation (5) for the stress, σ, without using any calibration factor. The predicted curves in Figure 6 follow the data closely, except at very low temperatures, -200°C and -150°C (Figure 6a), where Jones et al. reported brittle fracture with sharp elongation drops; and at -130℃ for the data in Figure 6b. From Figure 6a, the predicted values are very close to the measurements in the temperature range -100°C to 100°C. From Figure 6b, the agreement is very good from -60°C to 150°C, with maximum errors of -13% at -60°C and +24% at 150°C.

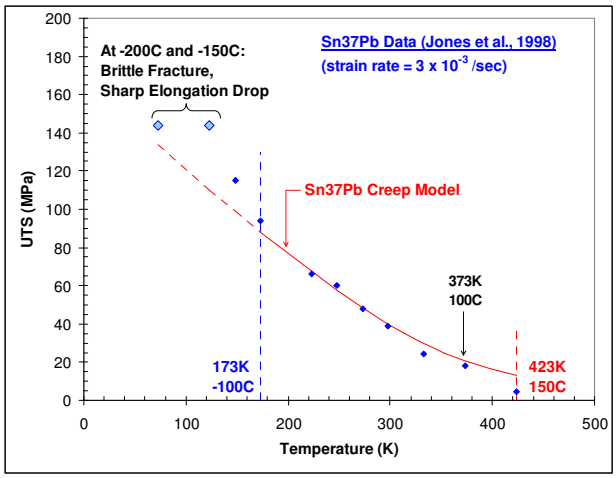

(a)

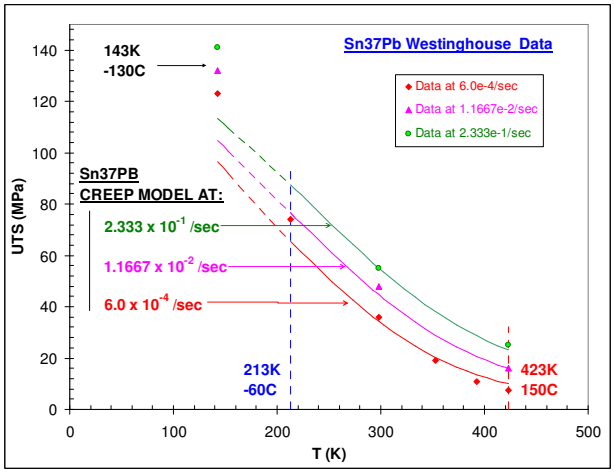

(b)

Figure 6: Predictions (lines) of 63Sn37Pb Ultimate Tensile Strength (UTS) versus temperature, using the 63Sn37Pb two-cell, creep model without calibration factor: (a) data at a strain rate of 3 x 10^{-3} / sec from Figure 2 in Jones et al. (1998); (b) Westinghouse data at three different strain rates from tables in DeVore et al. (1981).

The creep rate model given by equation (5) predicts UTS values rather well over the temperature range -55°C to 125°C, which is the usual range of interest for near-eutectic SnPb solder in electronics applications. This also suggests that near-eutectic SnPb creeps at cold temperatures down to at least -60°C. The latter conclusion differs from statements in industry standards (IPC-SM-785) to the effect that standard SnPb becomes brittle at temperatures below -25°C. No supporting data or references are quoted in the standard documents.

Comparison to 60Sn40Pb Thermal Cycling Data

Figure 7 shows a hysteresis loop of average shear stress and strain in 60Sn40Pb solder joints of a chip carrier assembly subject to thermal cycling between -25°C and 125°C, with 5 hour ramps (ramp rate = 0.5°C/min) and 2 hour dwell periods on the cold and hot side of the cycle. Solder joints were 13 mil (0.28 mm) tall. The chip carrier land dimensions were 12 mil x 40 mil and the board pads were 12 mil x 20 mil. The reader is referred to Hall, 1984 for further details on the test vehicle and on the stress/strain measurement technique. The loop simulation, implemented in a spread-sheet, uses a small time-step algorithm described in Clech, 2004b. The constitutive model that was used here includes elastic deformations and steady-state creep. No attempt was made to include primary creep or time-independent plastic flow.

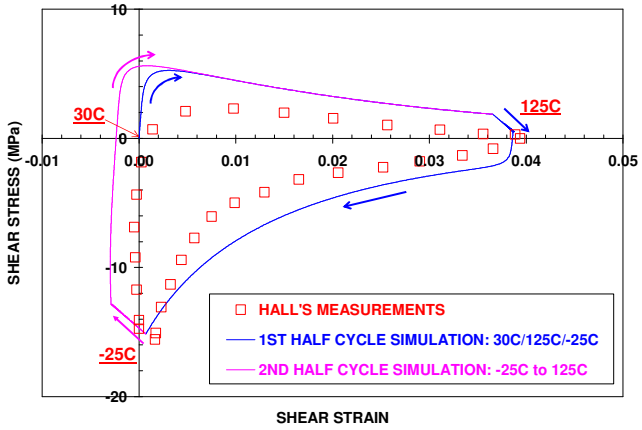

Figure 7: Stress/strain loop for 60Sn40Pb solder joints in shear during thermal cycling of a chip carrier board assembly. Data points are from Figure 9 in Hall, 1984. The simulation uses the 63Sn37Pb creep law given by equation (7) without calibration factor.

From equation (5), and assuming the Von Mises criterion applies, the steady-state creep rate in shear is given as:

$$\dot{\gamma}(/\sec) = \sqrt{3} \times \left\{ \begin{array}{l} 17.4\left(\tau\sqrt{3}\right)^{3.07} \cdot \exp\left[-\frac{7988}{T(K)}\left(1-\frac{\tau\sqrt{3}}{171}\right)\right] \\ +5112\left(\tau\sqrt{3}\right)^{5.89} \cdot \exp\left[-\frac{13516}{T(K)}\left(1-\frac{\tau\sqrt{3}}{217}\right)\right] \end{array} \right\} \quad (7)$$

Equation (7) was used as is, without any calibration factor. The slope of isothermal stress reduction lines at -25°C and 125°C was set to an average value |κ| = 644 MPa. The step-by-step simulation starts with an assumed, stress-free condition at the beginning of the first cycle (zero stress and strain at 30°C). The first half of the cycle, ramping up from 30°C to 125°C, followed by a 5 hour dwell at 125°C, and back down to -25°C, is highlighted as a long-dashed, blue line in Figure 7. The second half cycle from -25°C (with a 2 hour dwell) to 125°C is shown as a solid, pink line. There was no need to simulate additional cycles since the loop closed at the end of the first two half-cycles. The simulation, based on the two-cell creep model derived from Shi et al.'s (2002) tensile creep data, captures the shape of the data loop. A better fit can probably be obtained by adding appropriate features to the constitutive model, as was done in Clech

(2004b), using the approximation of a two-cell power-law model with an additional time-independent plastic flow rule.

APPLICATION TO EUTECTIC SN-58BI

EUTECTIC SN-BI MODEL

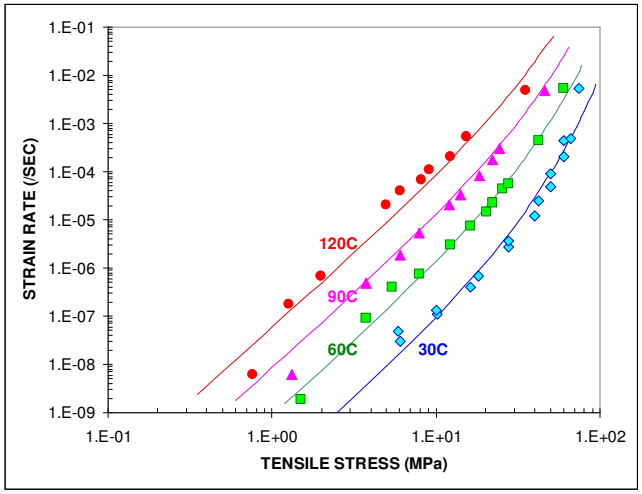

Figure 8: Sn58Bi steady state tensile creep data (symbols) from Figure 2 in Raeder et al., 1995, and fit of one-cell, obstacle-controlled creep model (solid lines).

Eutectic Sn58Bi has a fine lamellar microstructure with a Bi-rich phase (almost pure Bi) dispersed in a β-Sn matrix that contains small, round Bi precipitates (Seyyedi et al., 1993). The three-dimensional phases are almost continuous and bi-percolated due to almost equal volume fractions of Sn and Bi (Reynolds, 1998). Although creep of eutectic SnBi has been widely investigated, there are significant differences in creep activation energies and power-law exponents throughout the literature, and the mechanistic nature of creep mechanisms is not well understood (Glazer, 1994-95). Raeder et al. (1995) argue that Bi is the load carrying phase under low stress conditions ($\sigma < 3$ MPa) and that the higher modulus, Sn-rich phase is load-carrying and displays exponential creep in the high stress regime. Evidence of Sn-Sn and Sn-Bi boundary displacements was found in aged-coarsened specimens that underwent ageing for 22 days at 130°C, close to the melting point of 139°C. However, no grain boundary sliding was observed in unaged specimens. Mei et al.'s (1992) experiments led to one creep mechanism with an activation energy Q = 0.73 eV. Reynolds (1998) consolidated data from three experiments, including Mei et al.'s, and obtained creep activation energies: Q = 0.88 ± 0.02 eV in the low stress regime and Q = 0.95 ± 0.11 eV under high stress conditions. These two ranges of activation energies clearly overlap. Reynolds argues that two mechanisms operate in parallel based on power-law creep with different exponents in low and high stress areas. However, the physical basis of these creep mechanisms is not clear. Reynolds states that "*both are dominated by dislocation motion in the bulk, and are governed by an activation energy, Q, that is associated with lattice diffusion*". For quenched SnBi eutectic joints subject to shear in the approximate range: 4 to 12 MPa, Reynolds concludes that "*the rate controlling mechanism is not a grain boundary mechanism*".

Figure 8 shows the fit of a single-cell, obstacle-controlled creep model to the Sn58Bi creep data by Raeder et al. (1995) in the temperature range 30°C to 120°C. The equation of the solid lines is:

$$\dot{\varepsilon}(/\sec) = 802\sigma^{3.02} \cdot \exp\left[-\frac{9187}{T(K)}\left(1-\frac{\sigma}{596}\right)\right] \quad (8)$$

where σ has units of MPa. The central values and standard errors for the parameters in equation (8) are:

- Q_a = 76.4 ± 2.91 kJ/mole; m = 3.02 ± 0.14;
- σ_0 = 596 ± 97 MPa; A = 802 ± 798

The scaling constant A has the largest standard error. The correlation coefficient for fitting equation (4) to the 48 observation points in Figure 8 is r^2 = 97.7%.

- The apparent activation energy: Q_a = 76.4 kJ/mole = 0.79 eV is 9% higher than an activation energy of 70 kJ/mole (0.73 eV) in the single-mechanism power-law model by Mei et al. (1992). However, Q_a is 15% and 24% lower than Reynold's quoted values: Q = 0.88 eV in the low stress regime and Q = 0.95 eV under high stress conditions, respectively.
- The athermal flow strength of 596 MPa is 2.75 times higher than that of SnPb: σ_{02} = 217 ± 54 MPa in the matrix creep regime. The trend in flow strength parameters reflects the generally higher strength of eutectic SnBi compared to eutectic SnPb (Mei, 1992).
- The stress-exponent m = 3.02 is of the same order of magnitude as an exponent of 4.05 in the power-law model of Mei (1992) for eutectic SnBi in shear.

Last, note that, since the original data was in the temperature range 30°C to 120°C, there is no guarantee, without further verification, that the above Sn58Bi model would apply at cold temperatures.

MODEL TESTING

Comparison to Sn58Bi Shear Creep Rates

Assuming that Sn58Bi follows the Von Mises criterion, and substituting $\sigma = \tau \cdot \sqrt{3}$ and $\dot{\varepsilon} = \dot{\gamma}/\sqrt{3}$ into equation (8), the steady-state creep rate for eutectic SnBi in shear is obtained as:

$$\dot{\gamma}(/\sec) = 802\sqrt{3} \cdot \sigma^{3.02} \cdot \exp\left[-\frac{9187}{T(K)}\left(1-\frac{\tau\sqrt{3}}{596}\right)\right] \quad (9)$$

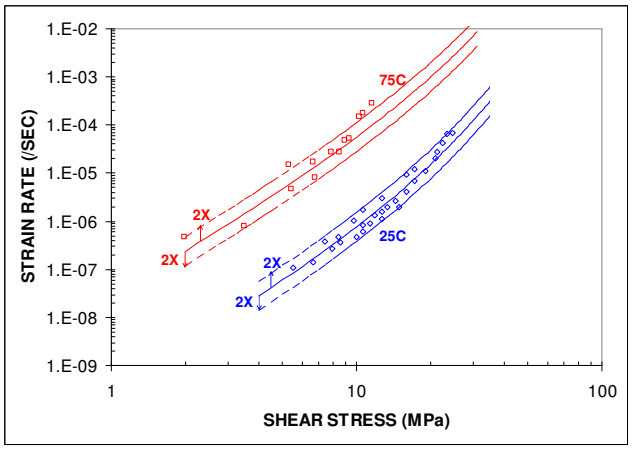

Figure 9: Fit of Sn58Bi creep model (solid lines) to Sn58Bi joint shear creep data (symbols) at 25℃ and 75°C. The data is from Figure 5.5 in Reynolds (1998).

Figure 9 shows shear creep data by Reynolds (1998) for eutectic SnBi joints with a solder pad area of 80mil x 45mil (2.03mm x 1.14mm) and thickness: 10 to 12mils (0.25 to 0.30 mm). The solder pads are two to four times larger than 1.27 mm pitch Ball Grid Array (BGA) pads with a typical diameter of about 20 mil. The joint thickness is representative of typical Chip Scale Package (CSP) solder joints. Without the use of a calibration factor, the model lines - given by equation (9) at 25℃ and 75°C - follow the data well. The data itself, 29 points at 25°C and 13 points at 75℃, shows a spread by a factor of about two times above and below the model lines.

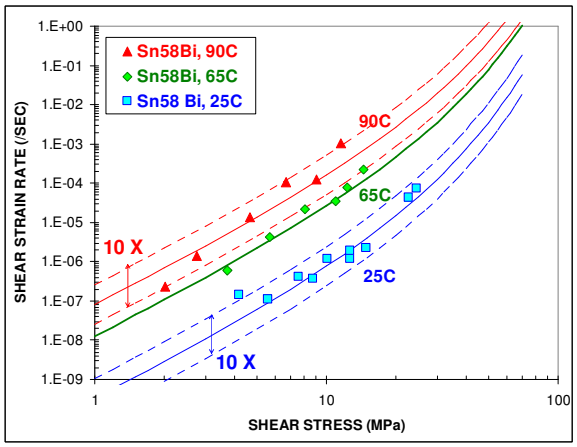

Figure 10: Fit of Sn58Bi creep model (solid lines) without calibration factor to Sn58Bi joint shear creep data (symbols) at 25℃, 65℃ and 90C°. The data is from Figure 5.5 in Hua et al. (1998).

Figure 10 shows the fit of the Sn58Bi creep model – equation (9) without any calibration factor - to another set of steady-state shear creep data in Hua et al. (1998) at room temperature (RT = 25℃), 65℃ and 90C°. At 65°C, the model fits the data quite closely. The RT and 90℃ data follow the model trend within a correlation band that is about one order of magnitude (10X) wide. That is, the data follows the model within a factor of √10 = 3.16 times above and below, which probably reflects some of the variability in steady-state creep rate measurements.

Comparison to Sn58Bi Shear Strength Data

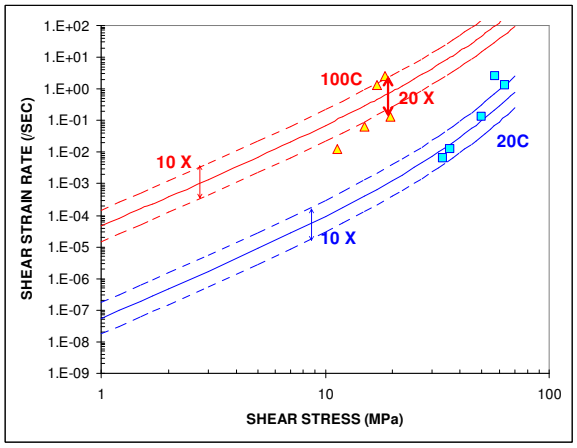

Figure 11: Fit of Sn58Bi creep model (solid lines) with a calibration factor C = 300 to shear strength data (symbols) for Sn58Bi copper ring and plug joints at 20℃ and 100C°. The data is from I.T.R.I. Publication No. 656.

Figure 11 shows the fit of the Sn58Bi creep model to shear strength data for tensional shear, copper plug and ring joints at 20℃ and 100°C (I.T.R.I Pub. No. 656). The shear strain rates were obtained by dividing the tensile test speed, given in mm/minute, by the joint thickness of 0.13 mm (5.12 mil). The solid lines in Figure 11 represent the shear creep rate equation for Sn58Bi - right hand-side of equation (9) - times a calibration factor, C. We obtained a visual best fit to the data in Figure 11 by using a multiplicative factor C = 300. The calibration factor is large, implying much higher strain rates than for small size, reflowed joints in Reynolds et al. (1998). In the case of plug and ring joints, which were formed by solder dipping, the joint length was 3.34 mm and the soldered joint area was large (100 mm^2 for a 9.52 mm plug diameter). After calibration, the model captures the trend in the shear strength data within approximately one order of magnitude (10X correlation bands in Figure 11). The raw data itself shows significant scatter by as much as 20 times as shown in Figure 11 for the high stress data points at 100℃.

APPLICATION TO EUTECTIC SN-0.7CU SOLDER

EUTECTIC SN-0.7CU SHEAR CREEP MODEL

The micro-structure of as-cast eutectic Sn0.7Cu (melting point = 227℃) typically features β-Sn dendrites and a Sn-rich matrix with tiny, spherical-like precipitates of Cu_6Sn_5 intermetallics, 0.5 μm or less in diameter (Wu et al., 2002). The intermetallic particles are finely dispersed and serve as discrete obstacles to dislocation motions. Thus,

the creep behavior of Sn0.7Cu is thought to be amenable to a one-cell, obstacle-controlled creep model.

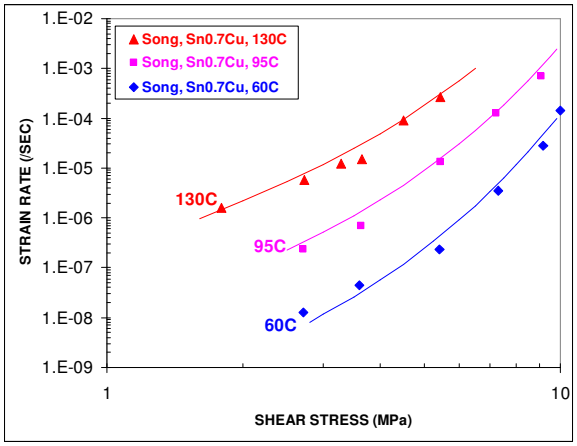

Figure 12: Sn0.7Cu steady-state shear creep data (symbols) from Figure 7c in Song et al., 2002a, and fit of a one-cell, obstacle-controlled creep model (solid lines).

Figure 12 shows the fit of a single-cell model to the Sn0.7Cu shear creep data by Song et al. (2002a) in the temperature range 60°C to 130°C. Note that the creep rates for the data in Figure 12, from Figure 7c in Song et al. (2002a), differ from creep rates from the same experiment in Figure 3c in Song et al. (2002b) by a factor of about 100 times. The correct rates are those in Figure 7c in Song et al. (2002a) as communicated by one of the authors (Hua, F., 2004).

The equation of the solid lines representing the single-cell model in Figure 12 is:

$$\dot{\gamma}(/\sec) = 2.23 \cdot 10^{8} \cdot \tau^{2.23} \cdot \exp\left[-\frac{14235}{T(K)}\left(1-\frac{\tau}{45.2}\right)\right] \qquad (10)$$

The central values and standard errors for the parameters in equation (10) are:

- Q_a = 118.3 ± 6.7 kJ/mole = 1.23 ± 0.07 eV;
- σ_0 = 45.2 ± 10.6 MPa (in shear);
- m = 2.23 ± 1.16; A = 2.13 x 10^8 ± 5.02 x 10^8

Again, the scaling constant A has the largest standard error. The correlation coefficient for fitting the model to the 17 observation points in Figure Z8 is r^2 = 97.4%. Comments on values of the physical parameters are:

- The apparent activation energy: Q_a = 118.3 kJ/mole = 1.23 eV is 23% higher than an activation energy of about 1 eV for tin self-diffusion. However, Q_a = 118.3 kJ/mole is quite close to an activation energy Q_{a2} = 112 ± 11 kJ/mole that was obtained earlier - equation (5) - for matrix creep in Sn37Pb solder.
- The athermal flow strength in shear is 45.2 MPa, 4.8 times lower than the value of 217 MPa for matrix creep in Sn37Pb solder. This is not surprising since creep rates for Sn-0.7Cu are quite similar to those of pure tin (Song et al., 2002 a & b) and eutectic SnPb has a higher strength than pure tin. At room temperature and at a strain rate of 5 x 10^{-3} /sec, Wu et al. (2002) reported a tensile strength of 37.5 MPa for pure Sn. Assuming that the Von Mises transformation applies, the equivalent shear strength is: 37.5 MPa / √3 = 21.65 MPa, that is, 2.1 times lower than the athermal flow strength in shear at 45.2 MPa.
- The stress-exponent: m = 2.3 is close to the theoretical value of 2 for alloys with small discrete obstacles.

MODEL TESTING: COMPARISON TO SN0.7CU TENSILE CREEP DATA

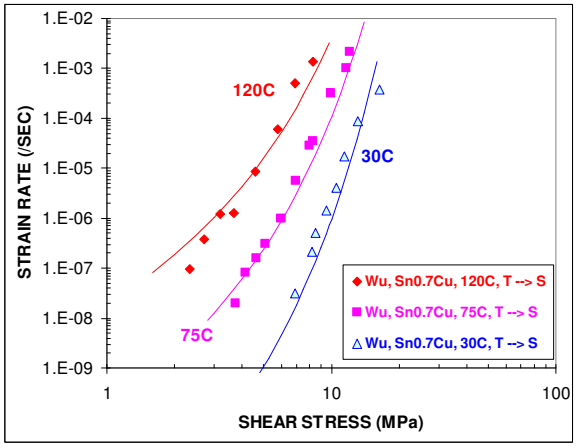

Figure 13: Fit of Sn0.7Cu shear creep model (lines) to Sn0.7Cu tensile data (symbols), using a model calibration factor: C = 0.2. The data is from Figure 4 and Table I in Wu et al. (2002). "T→ S" indicates tensile stress and strain rate were converted to their shear equivalents assuming a Von-Mises criterion.

Sn0.7Cu tensile creep data at 30°C, 75°C and 120°C from Wu et al. (2002) were converted to shear assuming the Von-Mises criterion applies: $\tau = \sigma/\sqrt{3}$, $\dot{\gamma} = \dot{\varepsilon}\cdot\sqrt{3}$. The data points are plotted in Figure 13 along with model lines using equation (10) with a multiplicative calibration factor C = 0.2. The fit is rather good, that is, the model follows the trends in the data well. The calibration factor C = 0.2 indicates that the Sn0.7Cu solder in the tensile specimens by Wu et al. (2002) was five times more creep resistant than the Sn0.7Cu solder joints in the experiment by Song et al. (2002a). This is probably the result of differences in microstructures (not documented in Song et al., 2002 a & b) which can be attributed to differences in specimen and process conditions, as summarized in Table 4. Note, in particular, that the shear joints were aged under harsher conditions and for a longer period of time than the tensile specimens. To put the Wu et al.'s aging conditions (2 hours at 100°C) in perspective, consider that Shohji et al. (2002) reported no significant difference in tensile strength of Sn3.5Ag and Sn3.5Ag0.75Cu after annealing specimens for 1 hour at 100°C.

APPLICATION TO SN4AG SOLDER

SN4AG TENSILE CREEP MODEL

As cast Sn4Ag solder (pasty range: 221-228°C) is near the eutectic alloy Sn3.5Ag (melting point: 221°C) and has a similar micro-structure featuring Sn dendrites and a Sn-rich matrix with dispersed Ag_3Sn intermetallics. Rhee et al. (2003) conducted isothermal stress-relaxation tests on Sn3.5Ag joints, revealing two temperature-dependent creep mechanisms: shear banding with deformations progressing through the grains at 25°C and 85°C, and grain boundary creep resulting in stress relief and decohesion at 150°C. In this section, we test the possibility of using a one-cell model for Sn4Ag, assuming that the stress-dependent true activation energy of the one-cell model – equation (3) – can possibly capture the two creep mechanisms reported by Rhee et al. (2003) for Sn3.5Ag joints. We also use a two-cell creep model - equation (4) - which would seem more appropriate for an alloy with distinct creep mechanisms. The two-cell model turns out to work best.

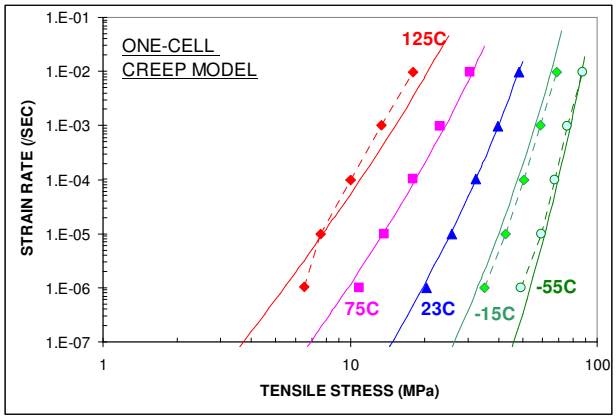

(a)

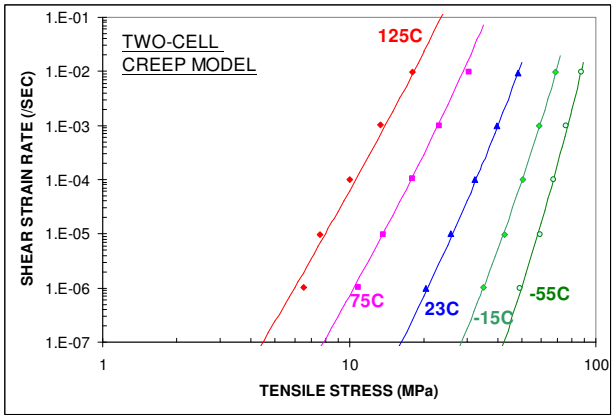

(b)

Figure 14: Sn4Ag tensile creep data (symbols) from Figure 10 in Neu et al. (2001) and obstacle-controlled creep model (solid lines) using: (a) a one-cell model: equation (11a); (b) a two-cell model: equation (11b).

Tensile creep data from isothermal strain rate jump tests on Sn4Ag specimens (Neu et al., 2001) were fit to one- and two-cell creep models. The raw data and the model lines are shown in Figures 14 a and b. The equation of the one- and two-cell creep models are:

$$\dot{\varepsilon}(/\sec) = 45.5\sigma^{5.63} \cdot \exp\left[-\frac{11028}{T(K)}\left(1-\frac{\sigma}{257}\right)\right] \quad (11a)$$

$$\dot{\varepsilon}(/\sec) = 2.77 \cdot 10^{-11}\sigma^{8.58} \cdot \exp\left[-\frac{6325}{T(K)}\left(1-\frac{\sigma}{244}\right)\right] + 67.3\sigma^{7.41} \cdot \exp\left[-\frac{12635}{T(K)}\left(1-\frac{\sigma}{408}\right)\right] \quad (11b)$$

Looking at Figures 14a, while the one-cell model seems to provide an overall decent fit, the model lines are at a slight departure from the data at -15°C and -55°C. More importantly, the model does not capture the trend of the 125°C data as reliably, with the model line clearly crossing over the data. The choice of a two-cell model is consistent with distinct creep mechanisms pointed out by Rhee et al. (2003) for Sn3.5Ag. The two-cell model fits the data much better (Figure 14b) with a correlation coefficient r^2 = 99.3% compared to r^2 = 96.0% for the one- cell model.

The central values and standard errors for the parameters in the two-cell model - equation (11b) - are:

- Q_{a1} = 52.6 ± 10.9 kJ/mole; m_1 = 8.58 ± 5.05; σ_{01} = 244 ± 154 MPa
- Q_{a2} = 105 ± 3.7 kJ/mole; m_2 = 7.41 ± 0.44; σ_{02} = 408 ± 82 MPa
- $A_1 = 2.77 \times 10^{-11} \pm 5.05 \times 10^{-10}$; A_2 = 67.3 ± 90.5

Comments on values of the physical parameters are:

- With the highest activation energy: Q_{a2} = 105 kJ/mole = 1.09 eV, close to the activation energy for tin self-diffusion, the second cell of the model (with subscript "2" for the parameters) is identified as representing matrix creep.
- With an activation energy: Q_{a1} = 52.6 kJ/mole = 0.55 eV, which is about half of Q_{a2}, the first cell of the model (with subscript "1" for the parameters) is identified as representing some kind of grain boundary creep.
- The athermal flow strength for matrix creep: σ_{02} = 408 ± 82 MPa is higher than values encountered thus far for matrix creep in Sn37Pb, Sn58Bi and Sn0.7Cu alloys. This is consistent with the generally higher strength of SnAg solders because of strengthening of the Sn-matrix by Ag_3Sn precipitates.
- The athermal flow strength for grain boundary creep: σ_{01} = 244 MPa is higher than that for grain boundary sliding in Sn37Pb (σ_{01} = 171 MPa). This can possibly be explained by strengthening of grain boundaries in Sn4Ag solder by small Ag_3Sn intermetallic precipitates.

- The parameters for the first cell (subscript "1") have large standard errors. This is possibly due to a lack of data in the high temperature region. The scaling constants A_1 and A_2 also have large standard errors possibly leading to unrealistic negative values which should be ignored.

MODEL TESTING: COMPARISON TO SN4AG STRENGTH DATA

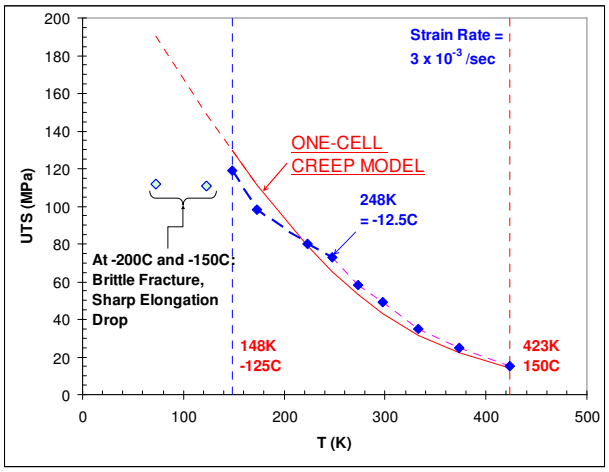

(a)

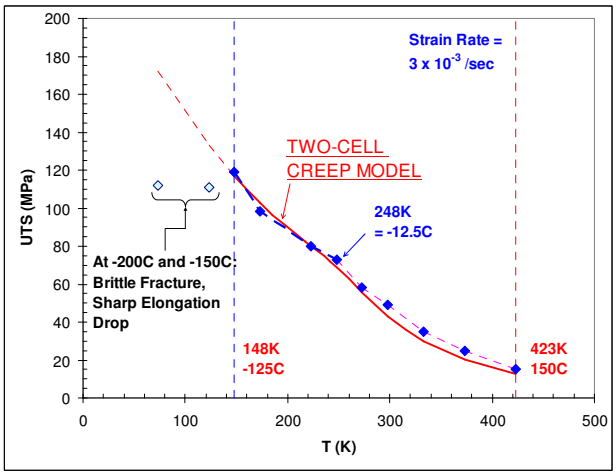

(b)

Figure 15: Sn4Ag tensile strength (UTS) data (symbols) versus temperature at a strain rate of 3 x 10^{-3} /sec and fit of (a) one-cell; (b) two-cell creep model with no calibration factor. The data is from Figure 2 in Jones et al. (1998).

Figure 15 shows Sn4Ag tensile strength versus temperature data (Jones et al., 1998) at a strain rate of 3 x 10^{-3}/sec. The predicted strength lines were obtained by back solving equations (11a) and (11b) – without any calibration factor - for stress at a given temperature in the range -200℃ to 150°C. The one- and two-cell models follow the trend of the UTS data in the temperature range -125℃ to 150°C quite well. At lower temperatures, both models are at a departure from the data. The creep-based models do not apply at -150℃ and -200℃ where the specimens were observed to fail in a brittle manner with a sharp drop in elongation characteristics. The good fit of the creep models to the data in the range -125℃ to 150℃ suggests that Sn4Ag creeps at cold temperatures down to -125°C.

A closer look at the data shows a small kink with a change of slopes in the data lines at about 248K (= -12.5℃). This does not appear to have been discussed by Jones et al. (1998) and it is not clear what the physics behind this change of slope is. The one-cell model curve in Figure 15a is very smooth and does not capture this effect. However, the two-cell model does, as can be seen in Figure 15b, suggesting that the change of slope may be related to interacting creep mechanisms at around 248 K (= -12.5℃). This would confirm, as discussed in the previous section, that a two-cell model is more appropriate for Sn4Ag solder.

APPLICATION TO EUTECTIC SN3.5AG SOLDER

EUTECTIC SN3.5AG SHEAR CREEP MODEL

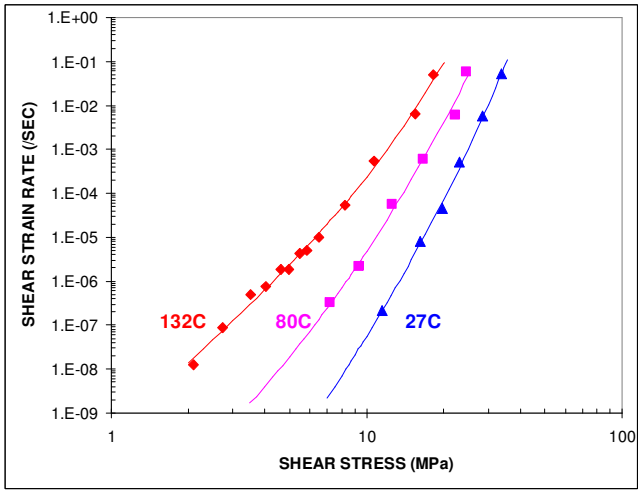

Figure 16: Fit of two-cell creep model (solid lines) to shear creep data (symbols) from isothermal creep tests on solder joints of Ceramic Chip Carrier (CCC) assemblies. The data is from Figure 17 in Darveaux et al., 1992.

Isothermal shear creep data from tests on Sn3.5Ag solder joints (Darveaux et al., 1992) were fit to a two-cell creep model (Figure 16). We chose a two-cell model because of the two deformation modes documented by Rhee et al. (2003) for Sn3.5Ag solder. The equation of the model lines in Figure 16 is:

$$\dot{\gamma}(/\sec) = 5.46\cdot 10^{-3}\tau^{7.48}\cdot\exp\left[-\frac{9207}{T(K)}\left(1-\frac{\tau}{156}\right)\right]$$
$$+1.018\cdot 10^{7}\tau^{5.11}\cdot\exp\left[-\frac{15417}{T(K)}\left(1-\frac{\tau}{294}\right)\right] \quad (12)$$

where the shear stress τ has units of MPa. The data is for temperatures in the range 27℃ to 132°C, so there is no

guarantee, without further evaluation, that the model applies at lower or higher temperatures.

The central values and standard errors on the model parameters in equation (12) are:

- Q_{a1} = 76.5 ± 9.4 kJ/mole; m_1 = 7.48 ± 2.07; σ_{01} = 156 ± 63 MPa
- Q_{a2} = 128.2 ± 77.9 kJ/mole; m_2 = 5.11 ± 0.87; σ_{02} = 294 ± 539 MPa
- $A_1 = 5.46 \times 10^{-3} \pm 4.14 \times 10^{-2}$; $A_2 = 1.018 \times 10^{7} \pm 2.37 \times 10^{8}$

With a higher activation energy, the second term on the right hand side of (12) likely represents some type of matrix creep. Comments on physical parameters of the model are:

- When converted to tension, and assuming the Von Mises criterion applies, the athermal flow strength in shear (294 MPa for matrix creep) has an equivalent tensile value of 294 x √3 = 509 MPa. This is of the same magnitude as an athermal flow strength σ_{02} = 408 MPa for matrix creep of Sn4Ag in tension (see equation 10b).
- Similarly, for grain boundary creep - represented by the 1st term on the right hand side of (12) - the athermal flow strength in shear (156 MPa) has a tensile equivalent of 156 x √3 = 270 MPa, close to a central value of 244 MPa for Sn4Ag in tension - see equation (11b).
- The activation energy for grain boundary creep: Q_{a1} = 76.5 kJ/mole = 0.79 eV is 45% larger than in the case of Sn4Ag (Q_{a1} = 52.6 kJ/mole = 0.55 eV). However, based on standard errors, the lower bound Q_{a1} = 67.2 kJ/mole = 0.70eV for Sn3.5Ag is close to the upper bound value: Q_{a1} = 63.5 = 0.66eV for Sn4Ag.
- The activation energy for matrix creep: Q_{a2} = 128.2 kJ/mole = 1.33 eV is 22% larger than in the Sn4Ag case (Q_{a2} = 105 kJ/mole). However, it is very close to an activation energy of 1.34 eV for Sn3.5Ag solder (see Table 4.2 in Pao, 1997) based on stress relaxation data from hysteresis loops obtained during thermal cycling of double-beam shear specimens.
- Even though the model fits the data well, standard errors on σ_{01}, σ_{02} and Q_{a2} are large. This may be due to the fact that the creep data considered in this example covers a limited temperature range.

Note that the Sn3.5Ag shear creep model is based on fitting the two-cell creep model to a limited number of data points at temperatures of 27°C, 80°C and 132°C. Remarkably, and perhaps fortuitously, this Sn3.5Ag creep model appears to work quite well for the nine test cases presented in the next section. In general, we would recommend curve-fitting creep models to datasets that cover the largest possible temperature range, say, -55°C to 160°C.

MODEL TESTING

Comparison To Sn3.5Ag Shear Strength Data

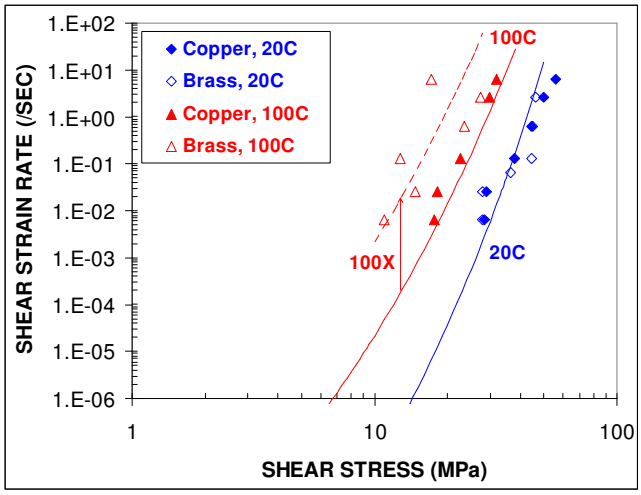

Figure 17: Plot of constant rate, shear strength data (symbols) at 20℃ and 100°C for Sn3.5Ag solder joints of copper or brass plug and ring specimens. The data is from tables, page 26 in I.T.R.I.'s Publication 656. The solid lines represent the two-cell shear creep model given by equation (12) without any calibration factor.

Figure 17 shows the fit of the Sn3.5Ag creep model – equation (12) with no calibration factor - to shear strength data for tensional shear, copper or brass plug and ring joints at 20℃ and 100°C (I.T.R.I Pub. No. 656). The test specimens were similar to those discussed earlier in the analysis of Sn58Bi shear strength data with a joint thickness of 0.13 mm (5.12 mil), a joint length of 3.34 mm and a soldered joint area of 100 mm^2 for a 9.52 mm plug diameter. For comparison purposes, the Sn3.5Ag creep equation (12) is based on shear testing of Darveaux et al.'s (1992) chip carrier solder joints with a 16-18 mil (~ 0.4 mm) height and 30 mil (0.762 mm) pad diameters. The joint thickness is similar in the two experiments but the soldered areas are widely different.

Without any calibration, the model follows the shear strength data well for the copper plug and ring joints at 20℃ and 100℃. The data for the brass plug and ring joints at 20℃ follows the copper plug and ring data and fits the model equally well. However, the 100℃ brass plug and ring data is offset from both the 100℃ copper plug and ring data and the 100℃ model line, by a factor of about 100 times. The reason for the offset of that particular dataset is not clear.

Comparison to Sn3.5Ag Shear Creep Data

Shear creep data (Kerr et al., 2004) from isothermal testing of lap shear specimens with 0.5 mm thick joints are shown in Figure 18. The specimens consisted of copper bars with a soldered area of about 1 mm^2. The reflowed specimens were air-cooled at a rate of 8.1℃/sec. The soldered joints in Kerr et al.'s (2004) specimens are

slightly taller than in Darveaux et al.'s (1992) ceramic chip carriers (0.5 mm vs. 0.4 mm) and the solder area is about twice as large (about 1mm^2 vs. 0.46 mm^2). With a calibration factor of 0.1 - multiplicative factor on the right hand-side of equation (12) - the model follows the general trend of the data although the model seems to deviate slightly from the 130°C data in the lower stress area. The creep rate data itself has a worst case scatter of one half- to one order of magnitude. The cooling rate was not documented in Darveaux et al.'s experiment, that in Kerr et al.'s is larger (8.1°C/sec) than in typical surface mount reflow profiles (1-3°C/sec).

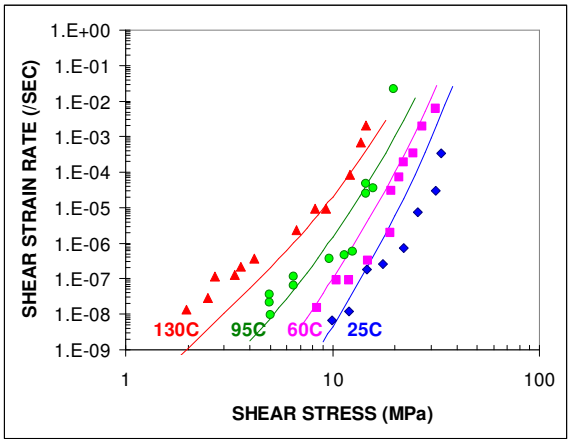

Figure 18: Plot of shear creep data (symbols) for Sn3.5Ag solder joints of lap shear specimens. The data is from Figure 2 in Kerr et al., 2004. The solid lines represent the shear creep model given by equation (12) with a multiplicative calibration factor C = 0.1.

Comparison To Sn3.5Ag Tensile Creep Data

Using the Von Mises transformation, equation (12) for creep of Sn3.5Ag in shear is converted to its tensile form as:

$$\dot{\varepsilon}(/\sec) = \left(\frac{1}{\sqrt{3}}\right)\times$$

$$\left\{\begin{array}{l} 5.46\cdot 10^{-3}\left(\sigma/\sqrt{3}\right)^{7.48}\cdot\exp\left[-\frac{9207}{T(K)}\left(1-\frac{\sigma/\sqrt{3}}{156}\right)\right] \\ +1.018\cdot 10^{7}\left(\sigma/\sqrt{3}\right)^{5.11}\cdot\exp\left[-\frac{15417}{T(K)}\left(1-\frac{\sigma/\sqrt{3}}{294}\right)\right] \end{array}\right\} \quad (13)$$

The model represented by equation (13) is plotted in Figure 19 against isothermal creep data from Schubert et al. (2001) and Huang et al. (2002). Information on the test specimens is summarized in Table 5. Process or aging information for the specimens by Schubert et al. (2001) was not available. In Figure 19a, we used a model calibration factor C = 3 - multiplicative factor on the right hand side of (13) - to provide a best visual fit to the data by Schubert et al. (2001). In Figure 19b with Huang et al.'s data (2003), the model lines were graphed as per equation (13) without any calibration factor. The difference in calibration factors is possibly due to differences in cooling rates. Measurements by Wu et al. (2003) indicate that creep rates for Sn3.5Ag can vary by one to two orders of magnitude depending on the cooling rate.

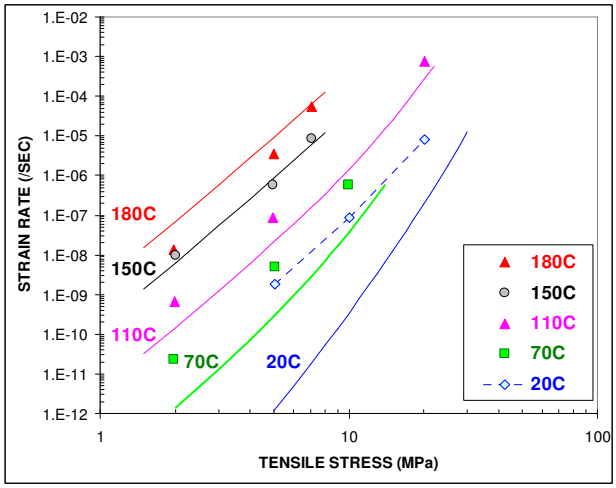

(a)

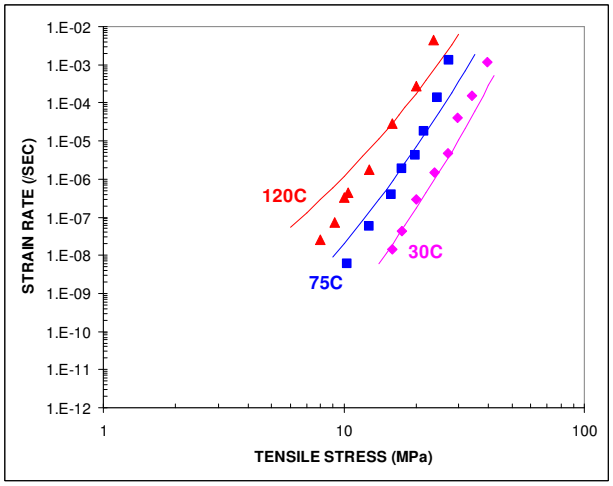

(b)

Figure 19: Sn3.5Ag tensile creep data and model lines as per equation (13): (a) Schubert et al.'s (2001) data and creep model with multiplicative calibration factor C = 3; data is from Figure 17 in Schubert et al. (2001); (b) Huang et al.'s (2002) data and creep model with no calibration factor; data is from Table I in Huang et al. (2003).

In Figure 19a, the model lines follow the data well, although with some scatter, at 110°C, 150°C and 180°C. The 70°C data displays a trend that is quite parallel to that of the model although the 70°C model line remains offset from the data by about one order of magnitude. The 20°C model line is offset from the 20°C data by as much as three orders of magnitude. However, the 20°C data itself is surprisingly close to the 70°C data, especially at the 5MPa stress level.

In Figure 19b, the non-calibrated model predicts the order of magnitude of creep rates well. The model follows the data closely at 30°C and 75°C. The 120°C data indicates a higher slope than predicted by the model. It is not clear why that is, given that the model follows the trends of stress / strain rate data from eight other experiments in this section on Sn3.5Ag.

Comparison to Sn3.5Ag Tensile Strength Data

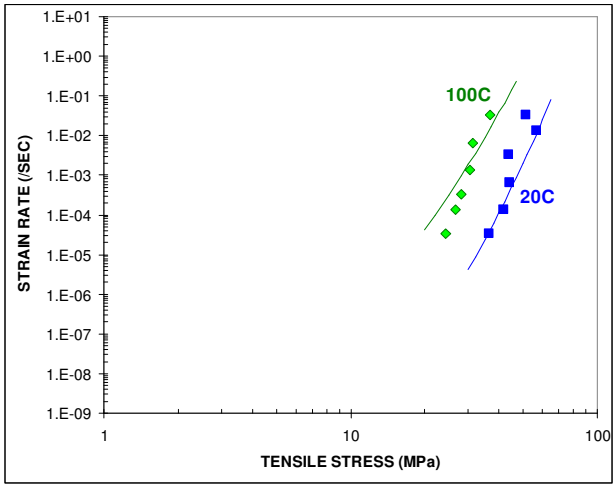

(a)

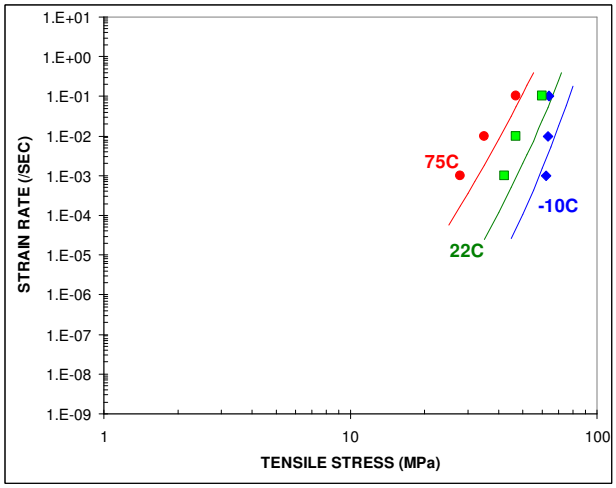

(b)

Figure 20: Model lines - equation (13) with no calibration factor - and tensile strength data at: (a) 20℃ and 100°C (data from the table, p. 24 , in ITRI Pub. # 656); (b) -10℃, 20℃ and 75°C (data from Figure 3b in Plumbridge et al., 1999).

Figure 20 shows the fit of the Sn3.5Ag tensile creep model - equation (13) with no calibration factor – to tensile strength data from constant rate stress/strain tests by I.T.R.I. and Plumbridge et al. (1999). Although the data at -10℃ and 20℃ shows some scatter, the non-calibrated model predicts tensile strength values reasonably well.

Comparison To Sn3.5Ag Compression Creep Data

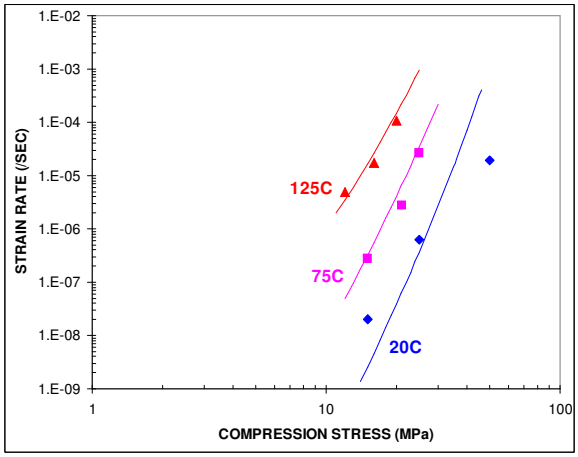

Figure 21: Model lines - equation (13) with multiplicative calibration factor C = 0.6 - and isothermal compression creep data for bulk Sn-3.5Ag solder (data is from NCMS Lead-Free Project Report).

Figure 21 shows steady-state creep data at 20°C, 75°C and 125°C from the NCMS compression creep tests on Sn3.5Ag cylindrical specimens - 0.4" (10.16 mm) in diameter x 0.8" (20.32mm) in length. Specimens were chill-cast after the specimens were heated up 40°C above the melting point of Sn3.5Ag (221°C). Using a multiplicative calibration factor C = 0.6 on the right hand side of equation (13), the Sn3.Ag tensile creep model captures the 75℃ and 125℃ data well. The 20℃ data shows some scatter around the 20°C model line.

Comparison to Sn3.5Ag Flip-Chip Shear Creep Data

The Sn3.5Ag shear creep model was bounced again flip-chip shear creep data by Wiese et al. (2001). The tiny, flip-chip solder joints of silicon-on-silicon Sn-3.5Ag assemblies were hour-glass shaped. Solder bumps were deposited using paste and processes from two manufacturers (labels: DG and PT in Figure 22). Pads were 0.1 mm x 0.1 mm or 0.2 mm x 0.2 mm and the hour-glass shaped solder joints were 0.15 mm or 0.2 mm in height. The average shear stress was defined as the applied force divided by the area of the minimum cross-section of the hour-glass shaped joints.

The steady-state creep data at 5℃ and 50°C for the DG paste joints are plotted in Figure 22a. The data at 10°C and 50°C for the PT paste joints are shown in Figure 22b. The model lines in Figures 22 a and b are from equation (12) with a multiplicative calibration factor C = 400 (DG paste) or C = 50 (PT paste). The model lines follow the trends in the data well. The use of a different calibration factor for the two paste types simply reflects the fact that the DG and PT joints creep at different rates. Comparing the 50°C data points in Figures 22 a and b, creep rates for the DG paste joints are about one order of magnitude higher than in the case of the PT paste joints.

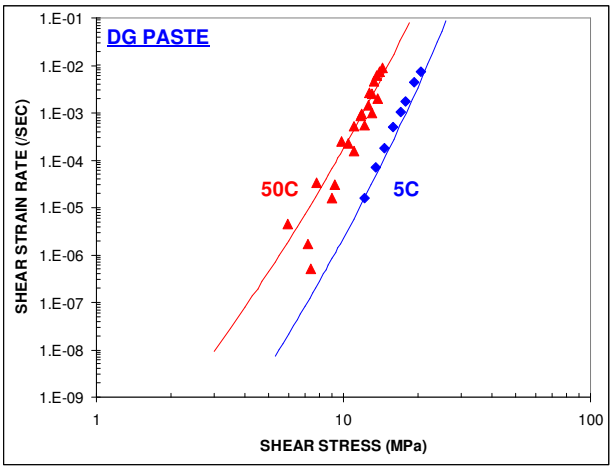

(a)

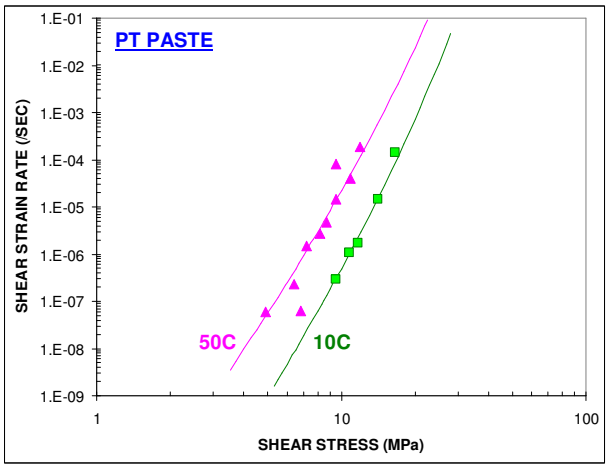

(b)

Figure 22: Sn3.5Ag flip-chip joint, shear creep data (symbols) from Figure 19 in Wiese et al. (2001): (a) DG paste data and model lines from equation (12) with a calibration factor C = 400; (b) PT paste data and model lines from equation (12) with a calibration factor C = 50.

Wiese et al. (2001) pointed out difficulties correlating bulk solder and flip-chip joint creep data when the data is analyzed using a power-law or hyperbolic sine model. Wiese et al. (2003) partially resolved that issue for Sn3.5Ag solder by using a two-cell power-law model for bulk solder while maintaining a single power-law model for the flip-chip data. However, the same approach did not seem to work when attempting the correlation of Sn-Ag-Cu creep data for bulk solder and flip-chip joints. It is remarkable that the two-cell obstacle-controlled model for Sn3.5Ag, obtained from chip-carrier solder joint creep data, captures the trend of the creep data for the Sn3.5Ag flip-chip joints. The calibration factors are high, suggesting an increase in the creep resistance of small volume flip-chip joints.

Comparison To Sn3.5Ag Thermal Cycling Stress/Strain Measurements

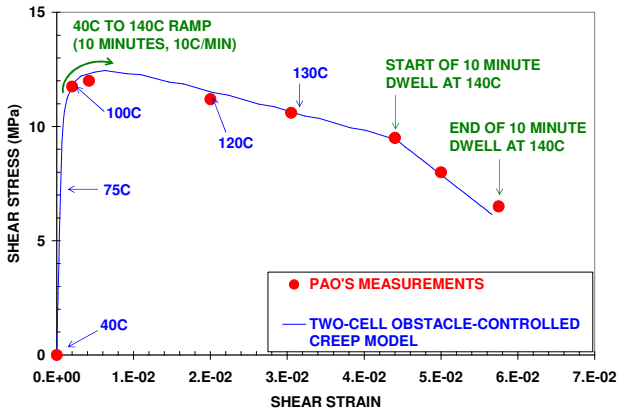

Figure 23: Measurements and simulation of the shear stress/strain response of Sn3.5Ag solder joints during thermal cycling of a double-beam (alumina on aluminum) test specimen. The data points are from Figure 4.3 in Pao (1997). The simulation uses the Sn3.5Ag shear creep model - equation (12) - with a calibration factor C = 22.

Figure 23 shows shear stress/strain measurements for Sn3.5Ag solder joints of a double-beam specimen subject to thermal cycling between 40°C and 140°C (10 minute ramp, 10°C/min rate, 10 minute dwell at 140°C). Solder joints were 0.381 mm thick, 2.0 mm long in the shear direction and 5.0 mm wide.

The model line uses the same algorithm as described earlier for the simulation of the Sn40Pb thermal cycling hysteresis loop. The slope of the isothermal stress reduction line at 140°C was set to $|\kappa|$ = 263 MPa. The solder constitutive model includes elastic deformations - with shear modulus in MPa: $\mu(T) = 18{,}623 - 66 * T(°C)$ - and steady-state creep rates given by equation (12) with a multiplicative calibration factor C = 22. The simulation follows the measurements closely and predicts stresses and strains accurately at the beginning and at the end of the 10 minute dwell period at 140°C.

APPLICATION TO SN3.8AG0.7CU

SN-3.8AG-0.7CU TENSILE CREEP MODEL

Isothermal creep data (Pang et al., 2003) from tensile tests on bulk Sn3.8Ag0.7Cu solder were fit to a two-cell, obstacle-controlled creep model (Figure 24). The data is for temperatures in the range -40°C to 125°C. Specimens had a 15 mm gauge length, were 3 mm in diameter and were aged for 24 hours at 60°C. The equation of the model lines in Figure 24 is:

$$\dot{\varepsilon}(/\sec) = 5.0\cdot 10^{-9}\sigma^{5.56}\cdot\exp\left[-\frac{3544}{T(K)}\left(1-\frac{\sigma}{1280}\right)\right] + 6802\sigma^{3.02}\cdot\exp\left[-\frac{11050}{T(K)}\left(1-\frac{\sigma}{181}\right)\right] \quad (14)$$

where the tensile stress σ has units of MPa.

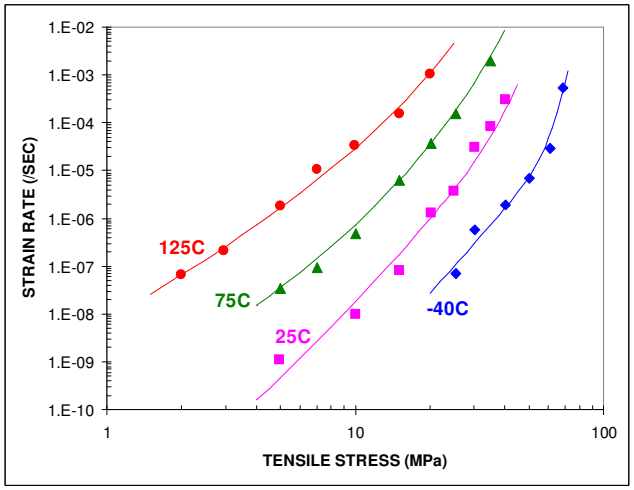

Figure 24: Fit of two-cell, obstacle-controlled creep model to Sn3.8Ag0.7Cu tensile creep data. The data is from Figure 1 in Pang et al., 2004. The model lines are given by equation (14).

The central values and standard errors on the model parameters are:

- Q_{a1} = 29.5 ± 6.9 kJ/mole; m_1 = 5.56 ± 0.88; σ_{01} = 1280 ± 4611 MPa
- Q_{a2} = 91.9 ± 7.6 kJ/mole; m_2 = 3.02 ± 0.25; σ_{02} = 181 ± 10 MPa
- A_1 = 5.00 x 10^{-9} ± 1.90 x 10^{-8}; A_2 = 6802 ± 16820

With higher activation energy, the second term on the right hand side of (14) likely represents some type of matrix creep. Comments on physical parameters of the model are:

- The activation energy for the first mechanism (likely some type of grain boundary creep): Q_{a1} = 29.5 kJ/mole = 0.31 eV is 44% lower than in the case of Sn4Ag (Q_{a1} = 52.6 kJ/mole = 0.55 eV).
- The athermal flow strength σ_{01} = 1280 MPa is quite high, which suggest the possibility of strong boundaries. However, the standard error on σ_{01} is large.
- The activation energy for matrix creep: Q_{a2} = 91.9 kJ/mole = 0.95 eV is 9% less than in the Sn4Ag case (Q_{a2} = 105 kJ/mole).
- The athermal flow strength σ_{02} = 181 MPa is surprisingly lower than a value of σ_{02} = 408 MPa for Sn4Ag.
- Even though the model fits the data well, standard errors on A_1 and A_2 are large, as is often the case with scaling constants of creep models.

Further modeling of creep data for Sn-Ag-Cu alloys of different compositions will help put the values of the above parameters in perspective.

MODEL TESTING

Comparison to Sn3.8Ag0.7Cu Shear Strength Data

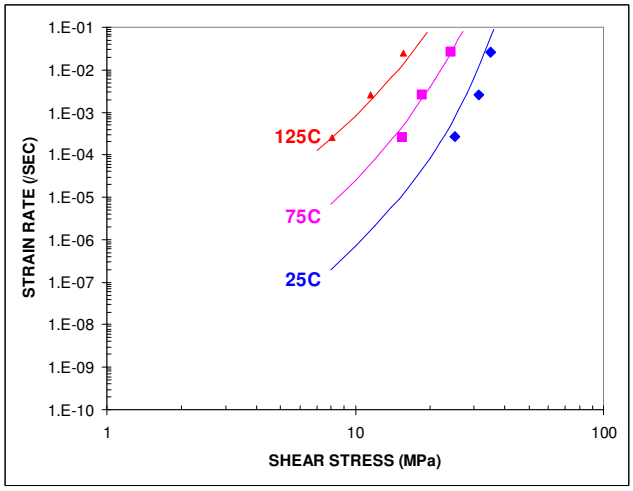

Figure 25: Fit of Sn3.8Ag0.7Cu model – equation (15) with no calibration factor – to shear strength data from Pang et al. (2003) at 25°C, 75°C and 125°C.

Figure 25 shows the fit of the Sn3.8Ag0.7Cu model to constant strain rate shear strength data by Pang et al. (2003). Assuming the Von Mises criterion applies, the model lines are given by the shear version of equation (14), i.e.:

$$\dot{\gamma}(/\sec) = \sqrt{3}\times \left\{ 5.0\times 10^{-9}\left(\tau\sqrt{3}\right)\sigma^{5.56}\cdot\exp\left[-\frac{3544}{T(K)}\left(1-\frac{\tau\sqrt{3}}{1280}\right)\right] + 6802\left(\tau\sqrt{3}\right)^{3.02}\cdot\exp\left[-\frac{11050}{T(K)}\left(1-\frac{\tau\sqrt{3}}{181}\right)\right] \right\} \quad (15)$$

The data is from shear lap joints simulating barrel-shaped solder joints of Chip Scale Package (CSP) assemblies. The joint dimensions were 0.32 mm height and 0.4 mm pad diameter. The assembly was 0.5 mm thick FR-4 on FR-4 with NiAu finish on the copper pads. The model lines in Figure 25 are obtained by using equation (15) without any calibration factor. The results indicate an excellent fit of the model to the shear strength data, also suggesting a good correlation between creep data and strength measurements as pointed out by Pang et al.

Comparison To Sn3.8Ag0.7Cu Shear Creep Data

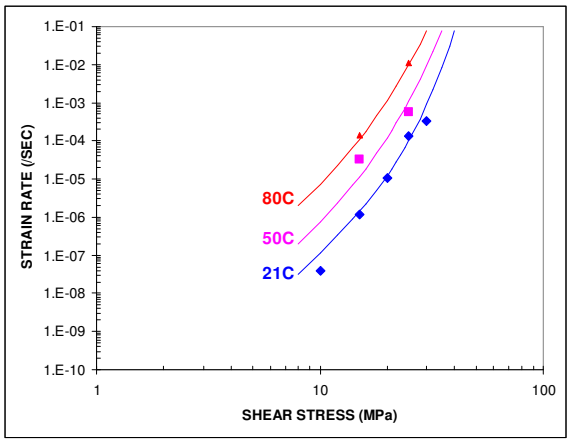

Figure 26: Fit of Sn3.8Ag0.7Cu creep model to Sn3.8Ag0.7Cu shear creep data by Dušek et al. (2003) at 21°C, 50°C and 80°C. The model lines are after equation (15) with a calibration factor C = 0.2.

Figure 26 shows a similar fit of the model to Sn3.8Ag0.7Cu shear creep data. Here, the model - equation (15) – was adjusted with a multiplicative calibration factor C=0.2. Solder joints in the experiment by Dušek et al. (2003) were lap joints in a copper fork specimen. Joint dimensions were 0.4 mm height, 2 mm length and 2 mm width. The specimen were "blow-torch" soldered, which probably resulted in differences in microstructural features when compared to the CSP type of joints used by Pang et al. (2003) for shear strength measurements. Nevertheless, with the use of a calibration factor, the model follows the trends of the shear creep data well.

Comparison To Sn3.8Ag0.7Cu Tensile Creep and Strength Data

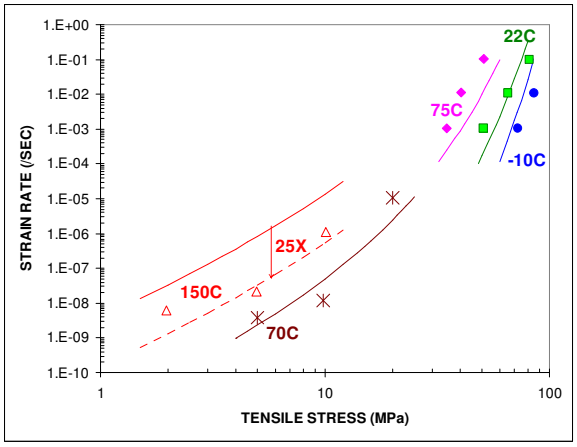

Figure 27: Fit of Sn3.8Ag0.7Cu tensile creep model to Sn3.8Ag0.7Cu tensile strength data by Kariya et al. (2001) and tensile creep data by Schubert et al. (2001). The model lines are after equation (14) with a calibration factor C = 0.1.

Figure 27 compares the Sn3.8Ag0.7Cu model lines to tensile strength data (Kariya et al., 2001) at -10°C, 22°C and 75°C, and tensile creep data (Schubert et al., 2001)) at 70°C and 150°C. All model lines are after equation (14) with a single calibration factor C = 0.1. Under high stress conditions (upper right of Figure 27), the model follows the trend of the tensile strength data. The model also shows continuity from high to low stress conditions and follows the trend of the 70°C creep data well. However, at 150°C, the model line is offset from the Schubert et al.'s data by a factor of about 25 times. Nevertheless, the trend of the 150°C model line and that of the data remain parallel. It is not clear why there is such an offset. Note also that the same experiment by Schubert et al. (2001) included creep data at 20°C - not shown here - which, surprisingly, was very close to the 70°C data.

Comparison To Sn3.9Ag0.6Cu Compression Creep Data

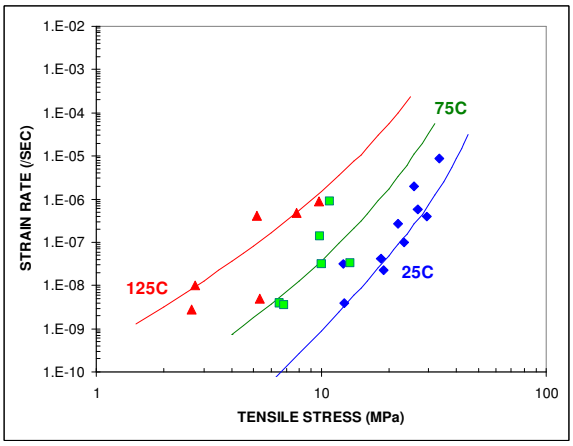

(a) at 25°C, 75°C and 125°C;

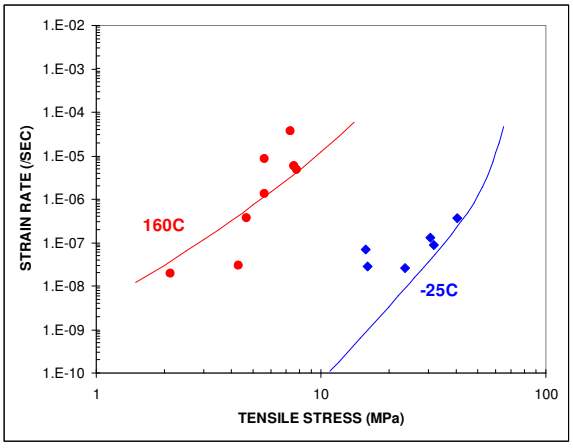

(b) at -25°C and 160°C

Figure 28: Fit of Sn3.8Ag0.7Cu tensile creep model to Sn3.9Ag0.6Cu compressive creep data by Vianco et al. (2004). The model lines are after equation (14) with a single calibration factor C = 0.05.

Assuming that the sensitivity of creep rates to alloy composition is a second order effect for small variations

in Ag and Cu contents, Figure 28 shows the fit of the Sn3.8Ag0.7Cu tensile model – equation (14) - to Sn3.9Ag0.6Cu compressive data by Vianco et al. (2004). The specimens that are referred to here were in the as-cast condition. With a single calibration factor C = 0.05, the model predicts the general magnitude of the Sn3.9Ag0.6Cu compressive data. For example, the model line at 25°C (Figure 28a) follows the trend in the data well. The data at 160°C (Figure 28b) would appear to follow a trend with a higher slope than predicted by the model, however, this could also be due to scatter in the creep data. Looking at the 75°C and 125°C data in Figure 28a indicates that scatter in the data can be as high as one or two orders of magnitude. At the time of this writing, we were unable to find Sn3.9Ag0.6Cu tensile creep data for a direct comparison to the Sn3.8Ag0.7Cu tensile creep model.

Last, note that the model calibration factor for the Sn3.9Ag0.6Cu compression creep data is small, C = 5 x 10^{-2}, and is of the same order of magnitude as a calibration factor C = 9 x 10^{-3} for the Sn40Pb compressive stress relaxation data in Figure 5. The smallness of these calibration factors is not related to the compressive nature of the data alone since, for Sn3.5Ag in compression, the model calibration factor was C = 0.6. At the other extreme, for Sn3.Ag flip-chip shear creep data, the model calibration factor was as high as 400. The range of calibration factors for the different alloys and specimen conditions is huge. This suggests that more attention needs to be paid to verifying the applicability of creep models to solder joints of real board assemblies.

APPLICATION TO OTHER LEAD-FREE SOLDERS

Figure 29 shows tensile creep data and model lines for two other lead-free solders: Sn3.5Ag0.75Cu and Sn2.5Ag0.8Cu0.5Sb.

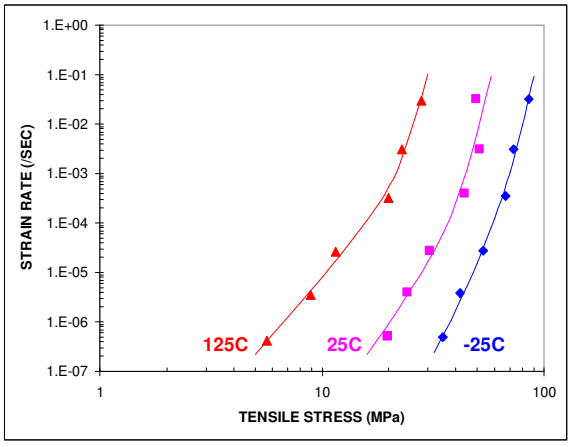

(a) Sn3.5Ag0.75Cu solder

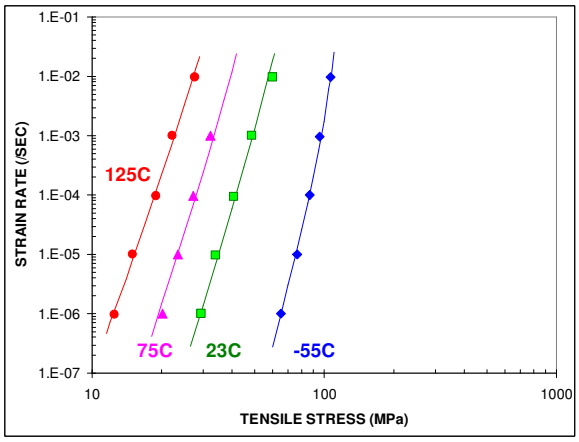

(b) Sn2.5Ag0.8Cu0.5Sb solder

Figure 29: Fit of two-cell, obstacle-controlled creep models to tensile creep data for (a) Sn3.5Ag0.75Cu solder, data from Amagai et al. (2002); (b) Sn2.5Ag0.8Cu0.5Sb solder, data from Neu et al. (2001).

The equations of the model lines for Sn3.5Ag0.75Cu and Sn2.5Ag0.8Cu0.5Sb are, respectively:

$$\dot{\varepsilon}(/\sec) = 2.48\cdot 10^{-2}\sigma^{4.69}\cdot\exp\left[-\frac{7778}{T(K)}\left(1-\frac{\sigma}{280}\right)\right] + 3.53\cdot 10^{-9}\sigma^{15.56}\cdot\exp\left[-\frac{14771}{T(K)}\left(1-\frac{\sigma}{840}\right)\right] \quad (16)$$

$$\dot{\varepsilon}(/\sec) = 1.53\cdot 10^{-9}\sigma^{11.35}\cdot\exp\left[-\frac{9834}{T(K)}\left(1-\frac{\sigma}{704}\right)\right] + 2397\sigma^{8.72}\cdot\exp\left[-\frac{18110}{T(K)}\left(1-\frac{\sigma}{301}\right)\right] \quad (17)$$

The correlation coefficients were r^2 = 97.4% for Sn3.5Ag0.75Cu and r^2 = 99.2% for Sn2.5Ag0.8Cu0.5Sb. The second terms on the right hand sides of (16) and (17) give the highest activation energies and are thought to represent some type of a matrix creep mechanism. The activation energies corresponding to the creep rates given by the first and second terms of equations (16) and (17) are:

- Q_{a1} = 64.7 kJ/mole = 0.67eV and Q_{a2} = 122.8 kJ/mole = 1.27 eV for Sn3.5Ag0.75Cu.
- Q_{a1} = 81.8 kJ/mole = 0.85eV and Q_{a2} = 150.6 kJ/mole = 1.56 eV for Sn2.5Ag0.8Cu0.5Sb.

The matrix creep activation energies, Q_{a2} 's, appear to be quite high. However, this is consistent with the effect of

Ag contents on apparent activation energies, as discussed in the next section. Due to time limitations and a lack of data, we were not able to bounce the above two models against independent datasets. Moreover, since the Sn3.5Ag0.75Cu model is based on a limited set of data in the temperature range 25°C to 125°C, the reader is advised to use that particular model with caution.

DISCUSSION

ALLOY COMPOSITION EFFECT

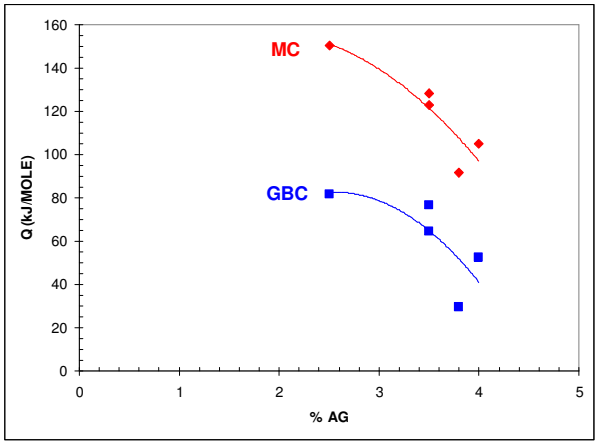

(a) %Ag effect

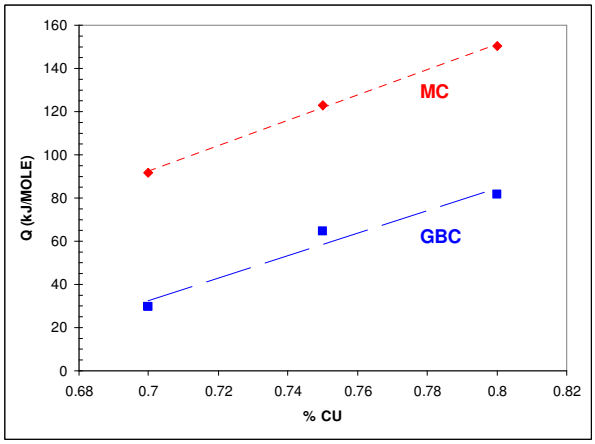

(b)%Cu effect

Figure 30: Alloy composition effect on Matrix Creep (MC) and Grain Boundary Creep (GBC) activation energies: (a) Ag contents effect for Sn2.5Ag0.8Cu0.5Sb, Sn3.5Ag0.75Cu, Sn3.5Ag, Sn3.8Ag0.7Cu and Sn4Ag solders;
(b) Cu contents effect for Sn2.5Ag0.8Cu0.5Sb, Sn3.5Ag0.75Cu and Sn3.8Ag0.7Cu solders.

Based on the physical parameters of two-cell, obstacle-controlled creep models for a variety of Sn-based, lead-free solders, apparent activation energies are plotted versus Ag and Cu contents in Figures 30 a and b, respectively. The two rates of the two-cell creep models are thought to represent some type of Grain Boundary Creep (GBC) and Matrix Creep (MC) mechanisms. Further metallurgical studies are needed to clarify the details of creep mechanisms for Sn-Ag-Cu solders. The data points in Figure 30a indicates that apparent creep activation energies increase with a reduced Ag contents in the range 2.5% to 4.0% Ag. The lowest values for the MC activation energies are in the range 95 to 105 kJ/mole, a range of activation energy that is often quoted for tin self-diffusion. The general trend in Figure 30a is that the MC activation energy for the Sn-Ag-Cu solders tends to be higher than for tin self-diffusion. This is probably a refection of the strengthening of the Sn matrix by Ag_3Sn and Cu_6Sn_5 precipitates. However, close to 4%Ag may lead to a reduction in creep resistance due to an excessive and detrimental amount of Ag_3Sn precipitates. This is consistent with creep rupture studies by Igoshev et al. (1999) where Sn4.0Ag was found to have shorter creep rupture lives (by about one order of magnitude) than Sn3.5Ag.

Both the GBC and MC curves in Figure 30a suggest that a reduced Ag contents (in the range 2.5% to 4%) provides for higher creep activation energies. This agrees with Sn2.5Ag0.8Cu0.5Sb (2.5% wt. Ag contents) being one of the most creep resistant solders among the alloys considered in this study. A much lower Ag contents may have a negative effect on creep resistance as suggested by much higher creep rates for Sn1.0A0.75Cu in Figure 1a. It appears that too low of a %Ag contents does not provide for enough dispersion-strengthening of the Sn-rich matrix. There is probably an optimum %Ag contents for improved creep resistance, perhaps somewhere near 2.5-3.5%Ag.

Figure 30b shows the effect of Cu contents on activation energies, based on the physical parameters for three Sn-Ag-Cu solders: Sn2.5Ag0.8Cu0.5Sb, Sn3.5Ag0.75Cu and Sn3.8Ag0.7Cu. The Cu contents is in the narrow range 0.7% to 0.8%. Within that range, activation energies appear to increase with Cu contents. However, since the Ag contents for the three alloys varies from 2.5% to 3.8% Ag, there may be hidden confounding effects not visible in the trends of Figure 30b. Further data points and a study of possible interaction effects are needed before conclusions can be drawn on the effect of Cu contents

CREEP MECHANISM CONTOURS

Sn37Pb Creep Contours

The two-cell creep models allow for the computation of strain rate contributions from the different creep mechanisms. Contour charts of MC versus GBC creep are developed to estimate the relative importance of both types of creep under a given set of stress and temperature conditions.

Creep mechanism contours are generated for a given percentage or ratio of creep rates for one mechanism over the total creep rates. Considering equation (5) for creep

of eutectic SnPb, the 75% GBS creep contour corresponds to stresses and temperatures for which the 1st term on the right hand side of (5) is 75% of the total creep rate. The creep contour lines for Sn37Pb are plotted in Figure 31.

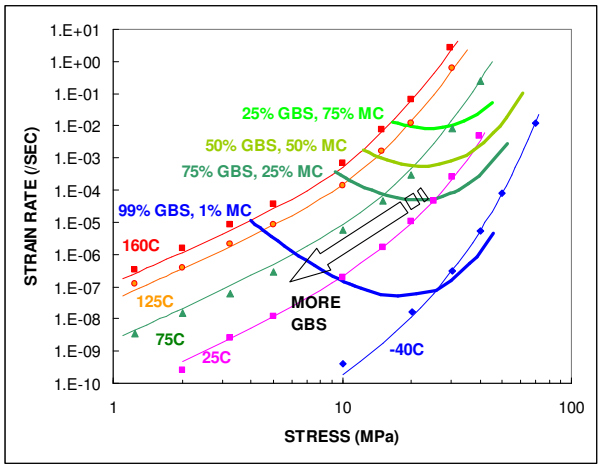

Figure 31: Sn37Pb tensile creep data and model lines (similar to Figure 3), and creep contour lines: %GBS and %MC are percentages of creep rate due to Grain Boundary Sliding (GBS) and Matrix Creep (MC).

The GBS and MC contour lines predict dominant GBS ("75% GBS, 25% MC" line in Figure F1) under low enough stress (under 10 MPa), and cold to high temperature (-40°C to 160°C), in agreement with observed creep mechanisms. For example, the metallurgical analysis conducted by Liu et al. (2003) on thermally-cycled (30°C to 125°C cycle, 1 hour ramp, no dwells) model 63Sn37Pb joints showed that solder cracking initiated within a couple of cycles. Micro-cracks initiated primarily at the boundaries between the Sn-rich and the Pb-rich phases, although some cracking occurred in the Sn- or Pb- rich phases as well. Under high stress (30 MPa) and elevated temperature (above 75°C), matrix creep dominates ("25%GBS, 75% MC" line in Figure 31). The above conclusions are similar to those obtained from creep contour charts developed by Grossmann et al. (2002) for creep of Sn36Pb2Ag solder using a two-cell power-law model.

Creep contour lines should be used cautiously. Although the shape of contour lines is not affected by creep rate calibration factors, the isothermal creep rate lines can shift up or down. The creep rate lines in Figure 31 are given by equation (5) with no calibration factor for Sn37Pb tensile specimens. These lines will be move up or down when a calibration factor is used for creep rate predictions to match measurements for other specimens or joints. This will change the relative percentage of creep mechanism contributions at a given temperature and stress level.

Sn3.8Ag0.7Cu Creep Contours

Figure 32 show creep contours for Sn3.8Ag0.7Cu solder. The isothermal creep rate lines are from equation (14) with a calibration factor C = 0.05 as in Figure 28 for fitting the Sn3.8Ag0.7Cu creep model to Sn3.9Ag0.6Cu compression creep data. This allows for a comparison of creep contours with results of the creep rate analysis and microstructural evaluation conducted by Vianco et al. (2004) on compression creep specimens. Here, the creep mechanisms are loosely labeled GBC and MC simply to distinguish the creep rate contributions from two mechanisms, the details of which are not fully understood yet. MC is for the creep rate component with the highest apparent activation energy in equation (14). GBC is for the creep rate component with the lowest apparent activation energy and does not necessarily refer to grain boundary sliding.

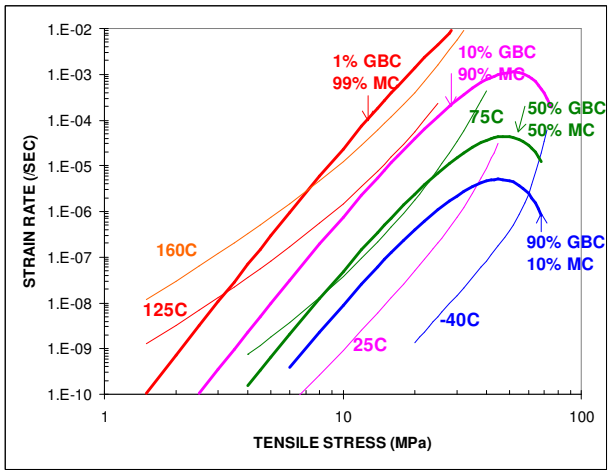

Figure 32: Sn3.8Ag0.7Cu contour lines (solid lines); isothermal creep rate lines (dashed lines) are given by equation (14) with a calibration factor C = 0.05 as in Figure 28 for Sn3.9Ag0.6Cu compression creep.

One of the interesting features of the Sn3.8Ag0.7Cu creep mechanism contours is that the contour line that gives equal contribution from the two creep rates ("50% GBC, 50% MC" line) is close to the 75°C creep rate line, at least up to about 25-30 MPa. This is the same temperature that Vianco et al. (2004) identified as the dividing point for the analysis of steady-creep rates, fitting the data with separate "sinh" models in the two temperature ranges: -25°C to 75°C, and 75°C to 160°C. More over, for specimens that were creep-tested at or above 75°C, the microstructural analysis of Vianco et al. (2004) revealed significant transformations within the inter-dendritic regions, namely, the formation of coarsened particle boundaries with depletion of Ag_3Sn precipitates in the vicinity of those boundaries. This mechanism was not observed in specimens tested at 25°C but was accentuated in specimens tested at 160°C. Since this mechanism occurred in the interdentritic regions, i.e. in the dispersion-strengthened Sn-matrix, the corresponding term in our creep contour analysis is

Matrix Creep (MC). In agreement with the microstructural analysis of Vianco et al. (2004), the creep contours indicate less than 10% MC at 25°C (at least up to 40 MPa), 50% MC at 75°C and more than 90% MC at 125°C and 160°C. Last, it is not clear yet to this author what the details of the second creep mechanism (labeled "GBC" in the creep contour chart) are. What we labeled GBC is not grain boundary sliding (as it was for Sn37Pb) since Vianco et al. (2004) indicated that no grain boundary sliding was observed in their metallurgical analysis of Sn3.9Ag0.6Cu compression creep specimens.

The pattern of creep contours in Figure 32 is quite different from that of creep contours for Sn37Pb (Figure 31), a reflection of vastly different creep mechanisms. While the Sn37Pb creep contour lines are kind of orthogonal to isothermal creep rate lines (at least for stresses less than 20 MPa), the Sn3.8Ag0.7Cu contour lines form less of an angle to, or are kind of parallel to the isothermal creep rate lines (up to about 20 MPa). This suggests that the areas of dominant creep mechanisms are highly temperature-dependent and that, in agreement with Vianco et al. (2004), the transition from one dominant creep mechanism to another occurs at a temperature within the range of common operating or accelerated testing conditions. This temperature-related transition implies that accelerated thermal cycling profiles should be designed carefully so that solder joint stress/strain cycles in test accelerate the same creep mechanism(s) as under service conditions. Solder joints for which the creep contours in Figure 32 apply would experience one dominant creep mechanism (labeled GBC in Figure 32) when thermally cycled between 25°C and 75°C but would experience both creep mechanisms (labeled GBC and MC in Figure 32) when thermally cycled between -40°C and 125°C under accelerated conditions. To this author's knowledge, the relative importance of competing creep mechanisms has not been addressed in the design of accelerated thermal cycling tests for lead-free solder assemblies.

USE OF OBSTACLE-CONTROLLED CREEP MODELS

The number of known and dominant creep mechanisms should dictate the choice of a one- or two-cell, obstacle controlled creep model. In the case of Sn0.7Cu, with dispersion-strengthening of the Sn matrix by fine intermetallic particles, a single-cell model was adequate although not much data was readily available to test the model over a wide range of circumstances. In the case of SnAg and SnAgCu solders, two-cell creep models appeared to work best. Two deformation modes have been identified for Sn3.5Ag (Rhee et al., 2003), but the details of creep mechanisms for other solders in the Sn-Ag-Cu family have not been fully elucidated yet.

Curve-fitting of two-cell, obstacle-controlled creep models involves the estimation of eight parameters. For ease of convergence of the non-linear regression procedure, the initial guess of physical parameters should be close to realistic values. Trends of activation energy as a function of Ag contents (Figure 30) may be of help in selecting initial values of apparent activation energies for Sn-Ag-Cu solders. For stress exponents, average values based on power-law models that are fitted to creep data in low and high stress regions may be of use as initial guesses. Initial values of athermal flow strength parameters were the most difficult to estimate. In a few cases, values based on the largest available strength measurements provided a good starting point.

In some cases, the data that we used for model fitting covered a limited range of temperatures. Ideally, models should be fitted to creep data over the largest possible range of interest, say, –55°C to 160°C for Sn-Ag-Cu solders. Once developed, creep models should be bounced against independent test results. For six of the solder alloys in this study, the creep models were bounced against a total of 23 datasets, that is, an average of almost four datasets for each solder alloy. Given the availability of creep data - or, sometimes, the lack of it! - testing or validation of creep models against at least three to four independent datasets seems like a reasonable target.

CONCLUSIONS

Obstacle-controlled creep models have been developed for Sn37Pb and seven lead-free solders: Sn58Bi, Sn0.7Cu, Sn3.5Ag, Sn4Ag, Sn3.8Ag0.7Cu, Sn2.5Ag0.8Cu0.5Sb and Sn3.5Ag0.75Cu.

- Except for the last two compositions, for which independent test data was not readily available, the models for the other six alloys were bounced against test results from independent laboratories. For the first six alloys, the models were tested against a total of 23 datasets.

- The obstacle-controlled creep models resolve many anomalies that have been observed in the analysis of lead-free solder creep data using power-law or "sinh" models. With the use of a simple, multiplicative calibration factor, the models allows for bridging tensile, shear and compression test results, as well as strength, creep and stress-relaxation data, and thermal cycling stress/strain measurements. In the case of Sn3.5Ag, the model allowed for bridging ceramic chip carrier joint creep data to flip-chip joint creep data in shear.

- While the models predict trends correctly, calibration factors were needed in 44% of the test cases (10 out 23 datasets). This suggests that it is important to verify the applicability of creep models and develop appropriate calibration factors before a particular creep model can be used in the stress/strain analysis of real solder joints. Thus, none of the models presented in this paper should

be used without verification that they apply to a given joint type. The most relevant test of a constitutive model, in this author's opinion, is the simulation of thermal cycling hysteresis loops from stress/strain measurements on soldered assemblies, as was done by Hall (1984) for Sn40Pb and Pao (1997) for Sn3.5Ag.

- For Sn-Ag or Sn-Ag-Cu alloys, a trend was observed showing that apparent creep activation energies increase with reduced Ag contents in the range 2.5% to 4% wt.

- One-cell creep models worked best for Sn0.7Cu and Sn58Bi, with stress exponents of 2.23 and 3.02, respectively. These exponents are close to the theoretical value of 2 in single-cell, obstacle-controlled rate-dependent plasticity models.

- The models for all other solder compositions are two-cell creep models with additive creep rates for separate creep mechanisms. This allows for the development of creep contour charts to identify stress and temperature conditions under which a given creep mechanism is dominant. Creep contour charts for Sn37Pb and Sn3.8Ag0.7Cu display vastly different patterns. The creep contour chart for Sn3.8Ag0.7Cu suggest a transition temperature for competing creep mechanisms at about 75°C, in agreement with the microstructural analysis of Vianco et al. (2004) on Sn3.9Ag0.6Cu compression creep specimens.

ACKNOWLEDGEMENTS

The author thanks Dr. Paul Vianco of Sandia National Laboratories for providing an early print of the paper by Vianco et al. (2004).

REFERENCES

[1] Amagai, M., Watanabe, M., Omiya, M., Kishimoto, K. and Shibuya, T., "Mechanical characterization of Sn-Ag-based lead-free solders", *Microelectronics Reliability*, Vol. 42, Issue 6, June 2002, pp. 951-966.

[2] Baker, E. and Kessler, T. J., "The influence of temperature on stress relaxation in a chill cast, tin-lead solder", *IEEE Transactions on Parts, Hybrids and Packaging*, Vol. PHP-9, No. 4, December 1973, pp. 243-246.

[3] Baker, E., "Stress relaxation in tin-lead solders", *Materials Science and Engineering*, Vol. 38, 1979, pp. 241-247.

[4] Bhadeshia, H. K. D. H. and Sourmail, T., "Design of creep-resistant steels: success & failures of models", *Japan Society for the Promotion of Science, Committee on Heat-Resisting Materials and Alloys*, Vol. 44, 2003, pp. 299-314.

[5] Clech, J-P., "Solder Reliability Solutions: a PC-based design-for-reliability tool", Proceedings, Surface Mount International Conference, Sept. 8-12, 1996, San Jose, CA, pp. 136-151 (available for download at http://jpclech.com). Republished in *Soldering and Surface Mount Technology*, Wela Publications, British Isles, Vol. 9, No. 2, July 1997, pp. 45-54.

[6] Clech, J-P., "Flip-chip / CSP assembly reliability and solder volume effects", Proceedings, Surface Mount International Conference, San Jose, CA, August 25-27, 1998, pp. 315-324 (available for download at http://jpclech.com).

[7] Clech, J-P., "Solder joint reliability of CSP versus BGA assemblies" (invited paper), Proceedings, System Integration in Micro Electronics, SMT ESS & Hybrids Conference, Nuremberg, Germany, June 27-29, 2000, pp. 19-28 151 (available for download at http://jpclech.com).

[8] Clech, J-P. (2004), "Lead-free and mixed assembly solder joint reliability trends", in Proceedings (CD-ROM), IPC / SMEMA Council APEX 2004 Conference, Anaheim, CA, Feb. 23-26, 2004, pp. S28-3-1 through S28-3-14. 151 (available for download at http://jpclech.com).

[9] Clech, J-P. (2004a), "Comparative analysis of creep data for Sn-Ag-Cu solder joints in shear", *Micromaterials and Nanomaterials* (IZM / MMCB publication, Fraunhofer Institute, Berlin, Germany), Issue 3, dedicated to the memory of Dr. Andreas Schubert, 2004, pp. 144-155 (available for download at http://jpclech.com).

[10] Clech, J-P. (2004b), "Review and analysis of lead-free solder material properties", chapter to appear in IEEE/Wiley book on NEMI's Lead-Free Project, 2004 (chapter can be viewed online at: http://www.metallurgy.nist.gov/solder/clech/ .

[11] Darveaux, R. and Banerji, K., "Constitutive relations for tin-based solder joints", *IEEE Transactions on Components, Hybrids, and Manufacturing Technology*, Vol. 15, No. 6, December 1992, pp. 1013-1024.

[12] Darveaux, R., "Effect of simulation methodology on solder joint crack growth correlation and fatigue life predictions", *ASME Transactions, Journal of Electronic Packaging*, September 2002, Vol. 124, No. 3, pp. 147-154.

[13] DeVore, J. and Westerman, L., *Solder and Solder Joint Properties Handbook*, GE Class 2, Syracuse, NY, September 1980.

[14] Dušek, M. and Hunt, C., "Measurement of materials properties of lead-free solders for modelling requirements", Proceedings (CD-ROM), SMTA International Conference, Chicago, IL, September 21-25, 2003.

[15] Dušek, M. and Hunt, C., "Do we know enough about lead free solders?", Proceedings, IPC/JEDEC 4th International Conference on Lead Free Electronic Assemblies and Components, Frankfurt, Germany, October 21-22, 2003, pp. 458-460.

[16] Frost, H. J. and Ashby, M. F., *Deformation Mechanisms Maps – The Plasticity and Creep of Metals and Ceramics*, Pergamon Press, 1982.

[17] Glazer, J., "Microstructure and mechanical properties of Pb-free solder alloys for low-cost electronic assembly: a review", *Journal of Electronic Materials*, Vol. 23, No. 8, 1994, pp. 693-700.
[18] Glazer, J., "Metallurgy of low temperature Pb-free solders for electronic assembly", IMR/273, The Institute of Materials and ASM International, 1995, pp. 65-93.
[19] Grivas, D., Murty, K. L. and Morris, J. W., "Deformation of Pb/Sn eutectic alloys at relatively high strain rates", *Acta Met.*, Vol. 27, 1979, pp. 731-737.
[20] Grossmann, G., Nicoletti, G. and Soler, U., "Results of comparative reliability tests on lead-free solder alloys", Proceedings (CD-ROM), 52nd Electronic Components and Technology Conference, San Diego, CA, May 28-31, 2002.
[21] Hall, P.M., "Forces, moments, and displacements during thermal chamber cycling of leadless ceramic chip carriers soldered to printed boards", *IEEE Transactions on Components, Hybrids and Manufacturing Technology*, 1984, Vol. 7, No. 4, Dec. 1984, pp. 314-327.
[22] Hua, F., Mei, Z. and Glazer, J., "Eutectic Sn-Bi as an alternative to Pb-free solders", Proceedings, 48th Electronics Components and Technology Conference, May 25-28, 1998, Seattle, WA, pp. 277-283.
[23] Hua, F., 2004, private communication.
[24] Huang, M. L. and Wang, L., "Creep behavior of eutectic Sn-Ag lead-free solder alloy", *Journal of Materials Research*, Vol. 17, No. 11, Nov. 2002, pp. 2897-2903.
[25] Igoshev, V. I., Kleiman, J. I., Shangguan, D., Wong, S. and Michon, U., "Fracture of Sn-3.5Ag solder alloy under creep", *Journal of Electronic Materials*, Vol. 29, No. 12, December 2000, pp. 1356-1361.
[26] IPC-SM-785, *Guidelines for Accelerated Reliability Testing of Surface Mount Solder Attachments*, November 1992.
[27] I.T.R.I., International Tin Research Institute, *Solder Alloy Data - Mechanical Properties of Solders and Solder Joints*, Greenford, Middlesex, UK, Publication No. 656, pp. 60-61.
[28] Jones, W. K., Liu, Y., Shah, M. and Clarke, R., "Mechanical properties of Pb/Sn, Pb/In and Sn-In solders", *Soldering and Surface Mount Technology*, Vol. 10, No. 1, February 1998, pp. 27-41.
[29] Kariya, Y. and Plumbridge, W. J., "Mechanical properties of Sn-3.0mass%Ag-0.5mass%Cu alloy", Proceedings, 7th Symposium on Microjoining and Assembly Technology in Electronics, Feb. 1-2, 2001, Yokohama, Japan, pp. 383-388.
[30] Kerr, M. and Chawla, N., "Creep deformation behavior of Sn-3.5Ag solder at small length scales", *JOM*, TMS, June 2004, pp. 50-54.
[31] Knecht, S. and Fox, L., "Integrated matrix creep: application to accelerated testing and lifetime prediction", Chapter 16, *Solder Joint Reliability: Theory and Applications*, ed. J. H. Lau, Van Nostrand Reinhold, 1991, pp. 508-544.
[32] Liu, X. W. and Plumbridge, W. J., "Damage produced in model solder (Sn37Pb) joints during thermomechanical cycling", *Journal of Electronic Materials*, Vol. 32, No. 4, April 2003, pp. 278-286.
[33] Mei, Z. and Morris, Jr., J. W., "Characterization of eutectic Sn-Bi solder joints", *Journal of Electronic Materials*, Vol. 21, No. 6, 1992, pp. 599-607.
[34] NCMS Lead Free Solder Project, National Center for Manufacturing Science, Report 0401RE96 (on CD-ROM), June 1998.
[35] Neu, R. W., Scott, D. T. and Woodmansee, M. W., "Thermomechanical behavior of 96Sn-4Ag and Castin Alloy", *ASME Transactions, Journal of Electronic Packaging*, Vol. 123, No.3, September 2001, pp. 238-246.
[36] Oakdale Engineering, Oakdale, PA, DataFit regression software, Version 7.1.
[37] Pang, J. H. L., Xiong, B. S., Neo, C. C., Zhang, X. R. and Low, T. H., "Bulk solder and solder joint properties for lead-free 95.5Sn-3.8Ag-0.7Cu solder alloy", Proceedings (CD-ROM), IEEE 53rd Electronic Components and Technology Conference, New-Orleans, LA, May 27-30, 2003.
[38] Pang, J. H. L., Xiong, B. S. and Low, T. H., "Creep and fatigue characterization of lead free 95.5Sn-3.8Ag-0.7Cu", Proceedings, 54th Electronic Components and Technology Conference, Las Vegas, NV, June 1-4, 2004, pp. 1333-1337.
[39] Pao, Y-H., "Design for Reliability", Chapter 4 in *Solder Joint Reliability of BGA, CSP, Flip Chip, and Fine Pitch SMT Assemblies*, J. H. Lau and Y-H. Pao, McGraw-Hill, 1997.
[40] Plumbridge, W. J. and Gagg, C. R., "Effects of strain rate and temperature on the stress-strain response of solder alloys", *Journal of Materials Science: Materials in Electronics*, No. 10, 1999, pp. 461-468.
[41] Raeder, C. H., Mitlin, D. and Messler, Jr., R. W., "Prediction of Two-Phase Creep Behavior from Constituent Phase Behavior in the Bi-Sn System", TMS Outstanding Student Paper Contest Winner, 1995 Undergraduate Division, on the web at: http://www.tms.org/Students/Winners/Raeder/raeder.html .
[42] Reynolds, H. L., "Creep of two-phase microstructures for microelectronic applications", Ph. D. dissertation, Engineering-Materials Science and Mineral Engineering, University of California, Berkeley, Fall 1998.
[43] Rhee, H. and Subramanian, K. N., "Effects of prestrain, rate of prestrain, and temperature on the stress relaxation behavior of eutectic Sn-3.5Ag solder joints", *Journal of Electronic Materials*, Vol. 32, No. 11, November 2003, pp. 1310-1316.
[44] Schubert, A., Walter, H., Dudek, R., Michel, B., Lefranc, G., Otto, J. and Mitic, G., "Thermo-mechanical properties and creep deformation of lead-containing and lead-free solders", Proceedings, 2001

International Symposium on Advanced Packaging Materials, pp. 129-134.
[45] Schubert, A., Dudek, R., Walter, H., Jung, E., Gollhardt, A., Michel, B. and Reichl, H., "Reliability assessment of flip-chip assemblies with lead-free solder joints", Proceedings (CD-ROM), 52nd Electronic Components and Technology Conference, San Diego, CA, May 28-31, 2002.
[46] Seyyedi, J., "Thermal fatigue behavior of low melting point solder joints", *Soldering and Surface Mount Technology*, No. 13, February 1993, pp. 26-32.
[47] Seyyedi, J., "Thermal fatigue of low-temperature solder alloys in insertion mount assembly", ASME EEP- Vol. 4-2, *Advances in Electronic Packaging*, Proceedings of the 1993 ASME International Electronic Packaging Conference, Binghamton, NY, September 29 - October 2, 1993, vol. 2, pp. 951-960.
[48] Shohji, I., Yoshida, T., Takahashi, T. and Hioki, S., "Tensile properties of Sn-3.5Ag and Sn-3.5Ag-0.75Cu lead-free solders", *Materials Transactions*, The Japanese Institute of Metals, Vol. 43, No. 8, 2002, pp. 1854-1857.
[49] Song, H. G., Morris, J. W., Jr. and Hua, F. (2002a), "Anomalous creep in Sn-rich solder joints", *Materials Transactions*, The Japan Institute of Metals, Special Issue on Lead-Free Electronics Packaging, Vol. 43, No. 8, pp. 1847-1853, 2002.
[50] Song, H. G., Morris, J. W., Jr. and Hua, F. (2002b), "The creep properties of lead-free solder joints", *JOM* (TMS), June 2002, pp. 30-32.
[51] Takahashi, H., Kawakami, T., Mukai, M., Mori, I., Tateyama, K. and Ohno, N., "Thermal fatigue life simulation for Sn-Ag-Cu lead-free solder joints", 2003 ICEP Proceedings, International Conference on Electronics Packaging, April 16-18, 2003, Tokyo, Japan, pp. 215-220.
[52] Vianco, P., "Creep behavior of the ternary 95.5Sn-3.9Ag-0.6Cu solder: Part I – As-Cast Condition", to appear in *Journal of Electronic Materials*, 2004.
[53] Wilshire, B., "Observations, theories, and predictions of high-temperature creep behavior", *Metallurgical and Materials Transactions A*, Vol. 33A, February 2002, pp. 241-248.
[54] Whitelaw, R. S., Neu, R. W. and Scott, D. T., "Deformation behavior of two lead-free solders: Indalloy 227 and Castin Alloy", *ASME Transactions, Journal of Electronic Packaging*, Vol. 121, No. 2, June 1999, pp. 99-107.
[55] Wiese, S., Schubert, A., Walter, H., Dudek, R., Feustel, F., Meusel, E. and Michel, B., "Constitutive behavior of lead-free solders vs. lead-containing solders - Experiments on bulk specimens and flip-chip joints", Proceedings, 51st Electronic Components and Technology Conference, Orlando, FL, 2001, pp. 890-902.
[56] Wiese, S., Meusel, E. and Wolter, K-J., "Microstructural dependence of constitutive properties of eutectic SnAg and SnAgCu solders", Proceedings, 53rd Electronic Components and Technology Conference, New-Orleans, LA, May 27-30, 2003, pp. 197-206.
[57] Wu, C. M. L. and Huang, M. L., "Creep behavior of eutectic Sn-Cu lead-free solder alloy", *Journal of Electronic Materials*, Vol. 31, No. 5, 2002, pp. 442-448.
[58] Wu, K. Wade, N., Cui, J. and Miyahara, K., "Microstructural effect on the creep strength of a Sn3.5Ag solder alloy", *Journal of Electronic Materials*, Vol. 32, No. 1, 2003, pp. 5-8.

AUTHOR'S BIOGRAPHY

Jean-Paul Clech is the founder and president of EPSI Inc. in Montclair, New-Jersey. His activities at EPSI include technical consulting for clients across the electronics industry, the development of design and reliability analysis tools, and professional training. He is the principal developer of the Solder Reliability Solutions model and application software, and has consulted on the physical design of a variety of components and small to large circuit boards. His research interests cover multi-disciplinary aspects of electronics packaging, Surface Mount Technology (SMT) and circuit board assemblies, with emphasis on materials characterization and the application of material science and mechanical engineering to sound product design. He is constantly challenged by design and reliability problems brought about by emerging packaging and soldering technologies and the application of SMT in harsh environments. His current technical interests are in the areas of flip-chip and chip scale package assemblies, lead-free properties and reliability, mechanical flexing and vibrations of circuit boards.

Jean-Paul previously was member of the technical staff at AT&T Bell Laboratories and manager of electronic packaging at a European super-computer start-up. He was trained as a metallurgist, receiving the "Diplôme d' Ingénieur" degree in the Materials Science Department at Ecole Centrale de Paris, France, and then as a mechanical engineer, receiving M.S. and Ph.D. degrees in the Mechanical Engineering Department at Northwestern University, Evanston, Illinois, where he worked on the mechanics and failures of hip and knee joint replacements. His interest in solder materials started during a post-doctoral assignment in the Materials Science department at Northwestern University. He is a recognized expert in the field of surface mount assembly quality and reliability and has assisted law firms as an expert witness on packaging, board and soldering related issues. Jean-Paul is an active member of ASME, IEEE, IMAPS, SMTA and TMS, has published over forty papers and has chaired numerous workshops and technical sessions at international conferences. He has been an invited speaker, lecturer and seminar leader at corporations, universities and R&D institutions in Asia, Europe and North America. In 2003, Jean-Paul received the SMTA Member of Distinction Award.

TABLES

Ref.	Solder Composition	Test Type	Specimen Geometry / Dimensions	Process / Treatment Conditions
Shi et al., 2002	63Sn37Pb	Tensile creep test	0.5 mm x 3 mm cross-section, 12 mm gauge length. H, 0.76 mm	Cast, air-cooled, machined. Aged: 24 hours at 60°C.
Whitelaw et al., 1999	60Sn40Pb	Tensile, strain-rate jump test	6.35 mm gauge section Ø, 12.7 mm gauge length	Cast, cooled at room temperature. > 3 weeks aging at room temperature

Table 1: SnPb creep test and specimen information.

Ref.	Solder Composition	Test Type	Specimen Geometry / Dimensions	Process / Treatment Conditions
Shi et al., 2002	63Sn37Pb	Constant load, tensile creep test	0.5 mm x 3 mm cross-section, 12 mm gauge length. H, 0.76 mm	Cast, air-cooled, machined. Aged: 24 hours at 60°C.
Baker et al., 1973	60Sn40Pb	Compressive stress relaxation test	12.7 mm (0.5") Ø, 50.8 mm (2") length	Cast in thin Teflon mold, cooled at room temperature (still air). 3 to 4 weeks aging at room temperature.

Table 2: Characteristics of SnPb creep and stress relaxation tests and test specimens.

Ref.	Solder Composition	Test Type	Specimen Geometry / Dimensions	Process / Treatment Conditions
Shi et al., 2002	63Sn37Pb	Constant load, tensile creep test	0.5 mm x 3 mm cross-section, 12 mm gauge length. H, 0.76 mm	Cast, air-cooled, machined. Aged: 24 hours at 60°C.
Jones et al., 1998	63Sn37Pb	Tensile test at constant strain rate	2 mm thick, 15 mm gauge length	Cast in water-cooled aluminum mold.
DeVore et al., 1980	63Sn37Pb	Tensile test at constant strain rate	1.4" (35.56 mm) gauge length, area: 0.1 in^2 .	Not available.

Table 3: Characteristics of Sn37Pb creep and constant strain rate tensile tests and test specimens.

Ref.	Solder Composition	Test Type	Specimen / Joint Geometry / Dimensions	Process / Treatment Conditions
Song et al., 2002	Sn0.7Cu	Creep of solder joints in shear	2.24 mm x 1.22 mm pads, 0.16 mm thick joints	Reflowed at 245°C, cooled at rate: 2.7°C/sec. Aged: 4 hours at 160°C.
Wu et al., 2002	63Sn37Pb	Tensile creep test	20 mm gauge length, 4 mm gauge diameter.	Chill-cast, cooled at about 1.5K/sec. Aged: 2 hours at 100°C.

Table 4: Characteristics of Sn0.7Cu creep tests and test specimens.

Ref.	Solder Composition	Test Type	Specimen / Joint Geometry / Dimensions	Process / Treatment Conditions
Schubert et al., 2001	Sn3.5Ag	Tensile creep test.	30 mm gauge length, 3 mm x 3 mm cross-section.	Not available
Huang et al., 2002	Sn3.5Ag	Tensile creep test	20 mm gauge length, 4 mm gauge diameter.	Cast, cooled at 8K/sec, aged: 2 hours at 100°C; machined.

Table 5: Characteristics of Sn3.5Ag tensile creep test specimens.